AN APPLICATION OF THE HILBERT TRANSFORM

TO THE MAGNETOTELLURIC METHOD

By

John E. Boehl, Francis X. Bostick, Jr., and Harold W. Smith

December 15, 1977

ELECTRICAL GEOPHYSICS RESEARCH LABORATORY

ELECTRICAL ENGINEERING RESEARCH LABORATORY

THE UNIVERSITY OF TEXAS AT AUSTIN

# ABSTRACT

Noise is inevitably encountered when the tensor magneto-telluric (MT) method is used for geophysical sounding purposes. Regardless of the source or nature of the noise, its effect is capable of altering the results given by the MT process. The tensor MT impedance estimates are affected in various ways depending on the character of the noise, the configuration of the source fields, and other factors.

It is shown that, for many cases, the magnitudes of the impedance elements are biased by noise on the MT data channels, whereas the phases of these elements are unbiased. A practical method for deriving or smoothing the amplitude data by phase imformation is presented in this report. The means for accomplishing this is based on the Hilbert Transform operation on minimum phase MT impedance functions. The formulas for the use of this method are developed, and some practical considerations are given for the implementation of the phase smoothing process. A theoretical model with and without synthetic noise is analyzed through this process to illustrate the validity of the technique. Also shown are several examples of results from this process as applied to actual tensor magnetotelluric impedance data.

# TABLE OF CONTENTS

## LIST OF FIGURES

# I. INTRODUCTION

The magnetotelluric (MT) method has become a valuable tool for determining the electrical properties of the subsurface structure of the earth. The first practical description of this method was set forth by Cagniard (1953). Critical evaluations of the method followed by others such as Wait (1954) and Price (1962), and so the evolution of the MT process began.

The Cagniard MT impedance functions are scalar relationships between the orthogonal electric (E) and magnetic (H) fields at the surface of the earth. These impedance functions have been subsequently modified to include the effects of two dimensional earth features. Cantwell (1960) proposed that when lateral inhomogeneities exist in the conductivity of the earth the MT impedance function should be represented as a rank two tensor. This concept has become the basis of the present MT method. Several people have studied the effects of various two dimensional models on the surface electromagnetic fields. These include d'Erceville and Kunetz (1962), Rankin (1962), Weaver (1963), Mann (1967), Geyer (1972), and Fischer (1975).

1

The list of people involved in the study of the tensor MT impedance method has steadily grown since the method was first formulated. Some of the investigations in this area are given by Bostick and Smith (1962), Swift (1967), Vozoff (1972), Hermance (1973), and several others listed in the next chapter.

The increase in interest of the Cagniard and tensor MT impedance methods for geophysical prospecting has been indicated by the large amount of experimental data presented in the literature. Several of the earlier reports of results from the MT process include those given by Vozoff, et. al. (1963) and Hopkins and Smith (1966). Among the many others who have reported the results of experimental MT surveys are Morrison, et. al. (1968), Dowling (1970), Word, et. al. (1970), Reddy and Rankin (1971), and Stanley, et. al. (1977). The references given here by no means represent a comprehensive list. The reader is referred to Hermance (1971) for additional information regarding the work done by others in the various areas of the magnetotelluric process.

From its infancy the MT method has presented many problems associated with noise. The overall value of results obtained from the MT process initially depends upon the quality of the original data. This in turn is determined not only by the characteristic noise level of the instrumentation system but also by the care with which

the data are acquired. Noise may also be introduced into the results during the analysis of the MT data (Sims and Bostick, 1969).

The amplitudes of the electric and magnetic fields which exist at the sensors during the course of MT data acquisition are normally very small. The E field fluctuations often require voltage measurements in the microvolt range while the magnetic field is only tens to hundreds of milligamma in magnitude. These low level signals require instrumentation (including sensors) which are characterized by very low noise levels.

The tensor MT impedance method as is was first used involved E and H field measurements in the frequency range of $10^{-3}$ or $10^{-4}$ Hz to about 10 Hz. Recent developments, however, have permitted the use of audio magnetotelluric (AMT) equipment capable of yielding tensor data at frequencies up to and above about 1 KHz (Grosskopf, et. al., 1974). Certain noise related problems exist in various segments of this extended frequency range and, therefore, must be dealt with if high quality data are to be realized.

One type of noise introduced by the instrumentation in the lowest portion of the frequency spectrum is a result of thermal effects on the magnetic field sensors. Thermal or chemical changes of the electric field sensors have also been observed to create noise in this frequency band.

Many problems are encountered when MT measurements are attempted throughout the central portion of the frequency spectrum (from about $10^{-1}$ Hz to 10 Hz). A major factor which causes this band to be the most difficult in the MT process is the extremely low signal level available. The power spectrum of the source magnetic field decreases sharply with respect to increasing frequency, approaching extremely low levels at about 0.1 Hz. Sources such as wind which cause even slight physical motions of low signal level portions of the MT equipment (induction magnetometers, cables, etc.) can induce noise in the midband of frequencies. This example of a noise source coupled with the normally low signal level can result in poor quality data unless low noise equipment is carefully used.

The upper portion of the frequency spectrum also presents unique problems when the AMT data acquisition process is attempted. A particular problem encountered in the upper band is a result of the impulsive nature of the AMT signal. The source field for this frequency band is the result of electrical discharges in thunderstorms. The nature of the signal imposes stringent dynamic range requirements on the AMT equipment. Saturations occurring in the electronic circuits due to large spikes at the input can result in noisy data for this band of frequencies. This non-linear type of

noise can severely corrupt the results.

Early MT equipment was noisy (as well as bulky) primarily due to the electronic devices available at the time. A generally primitive notion of the MT method also contributed to inconsistencies in the early results. Recent advances in semiconductor devices and careful design of the equipment cannot only reduce the size of the system but also provide lower levels of noise originating in the electronic circuits. The design and construction of such systems, however, require a familiar understanding of the tensor MT method and its associated problems. A knowledge of where noise is most likely encountered and the effects of this noise on the results of analysis is imperative for the design and use of high quality MT systems.

It is thus evident that noise can be introduced into the data from many sources and in many ways. In spite of the degree of sophistication possessed by the equipment and the care taken during the data acquisition and analysis processes, the effects of noise are often apparent on MT results. The purpose of this report is to describe and evaluate a method which has been utilized to extricate useful MT results from data corrupted by noise.

## II. BASIC TENSOR MT METHODS

The tensor magnetotelluric impedance method has been described by Cantwell (1960), Bostick and Smith (1962), Swift (1967), Sims and Bostick (1969), Word, et. al. (1970), and others. A very brief summary of some of the fundamentals of the method is given here so that notation subsequently used may be clearly defined. Details of the tensor method may be found in the references given above.

The tangential electric and magnetic fields at the surface of the earth are related by the tensor MT impedance as

$$[E] = [Z][H] \tag{2-1}$$

or

$$E_x = Z_{xx}H_{xx} + Z_{xy}H_y \tag{2-2}$$

and

$$E_y = Z_{yx}H_x + Z_{yy}H_y. \tag{2-3}$$

An alternate form relating the surface E and H quantities is given by the admittance tensor as

$$[H] = [Y][E] \tag{2-4}$$

where [Y] is the matrix inverse of [Z].

6

When MT data indicate that a two dimensional structure is present, the data are rotated to give the principal impedance functions $Z'_{xy}$ and $Z'_{yx}$. These are computed with axes parallel and perpendicular to the strike direction of the two dimensional feature (Word, et. al., 1970). The rotation angle which maximizes $|Z'_{xy}|^2 + |Z'_{yx}|^2$ or minimizes $|Z'_{xx}|^2 + |Z'_{yy}|^2$ locates the principal axes for this case.

For noise-free data from either a one dimensional earth or a two dimensional one with data rotated to the principal axes, the main diagonal elements of the impedance tensor theoretically vanish. The decoupled tensor equations then become

$$E'_x = Z'_{xy} H'_y \qquad (2-5)$$

and

$$E'_y = Z'_{yx} H'_x \qquad (2-6)$$

From these principal impedance values the apparent resistivities are calculated as

$$\rho_{xy} = \frac{1}{\omega\mu} |Z'_{xy}|^2 \qquad (2-7)$$

and

$$\rho_{yx} = \frac{1}{\omega\mu} |Z'_{yx}|^2 \qquad (2-8)$$

where $\omega$ is the radian frequency and $\mu$ is the permeability of free space. Associated with the apparent resisitivity values are the

phases of the principal impedances

$$\varphi_{xy} = \tan^{-1}\left(\frac{X'_{xy}}{R'_{xy}}\right) \qquad (2-9)$$

and

$$\varphi_{yx} = \tan^{-1}\left(\frac{X'_{yx}}{R'_{yx}}\right) \qquad (2-10)$$

where the R's and X's are the real and imaginary parts, respectively of the rotated impedance values.

The ultimate purpose of the MT process is to provide a geological model for the earth in terms of true resistivity at the measurement site. The apparent resistivity functions must therefore be converted to a true resistivity, spacially varying function for each MT site. Some three dimensional modeling schemes may be possible if measurements are made at a great number of closely spaced sites in a given region. For widely spaced sites, however, the only tractable methods which yield interpretable results are based on one dimensional inversion techniques. A number of methods have been used for one dimensional inversions including those given by Wu (1968), Becher and Sharpe (1969), Patrick and Bostick (1970), Nebetani and Rankin (1969), Laird and Bostick (1970), Johnson and Smylie (1970), and others.

For one or even two dimensional situations any of the inversion methods may be suitable for the resolution of the final MT

results. Many of these techniques, however, do require a huge amount of computing power. A greatly simplified process has been developed which does not require the extensive computing effort as do other methods (Bostick, 1977). This method does, however, require a smoothly varying (noiseless) apparent resistivity vs. log frequency function. The process outlined in this dissertation was developed partly to provide this needed function.

The sensitivities of the various inversion results to noise on the original data may vary from method to method. Regardless of the process used, however, the results are affected by noise to some degree. The quality of the final MT results can therefore be improved if the effects of noise on the tensor impedances can be reduced.

III.  NOISE AND THE TENSOR MT IMPEDANCE

A.  Bias of the Impedance Estimates

Each of the tensor impedance elements of Equations (2-2) and (2-3) may be derived in six ways, as discussed by Sims et. al. (1971). When noise is encountered during the acquisition of MT data, it affects the various estimates of the impedance elements in different ways. The manner in which the estimates are corrupted by noise depends on the many situations which may be encountered. Noise may exist on one or more channels of data and may be coherent between channels. The earth's structure at the point of measurement may be one, two, or three dimensional in nature. In addition to these factors, some undesirable features of the source field of the MT method may exist.

The many possible combinations of types of noise, earth structure, and incident field property make a detailed study of noise effects on the MT impedance difficult. The following discussion does not represent a comprehensive or quantitative analysis of these effects. It does, however, provide some brief qualitative observations so as to illustrate these effects on the estimates for a few limiting cases.

As indicated by Equations (2-7) and (2-8) the apparent resistivity is given by the square of the impedance magnitudes. Thus any noise on the impedance is accentuated on $\rho_{xy}$ or $\rho_{yx}$. As will be discussed in the next chapter, the apparent resistivity vs. frequency function may be derived, under certain assumptions, from the phase of the impedance function. The effects of noise on the phase of Z as well as on its magnitude will therefore be considered for the cases of interest here.

An insight into the manner in which the complex impedance estimates are affected by noise may be gained if certain simplifying assumptions are made with regard to the MT environment and the type of noise encountered. Although the following discussion is applicable to both the $Z_{xy}$ and $Z_{yx}$ elements of the tensor impedance (as well as to $Y_{xy}$ and $Y_{yx}$ of the tensor admittance), only $Z_{xy}$ will be considered for the sake of brevity.

Three cases are considered here with varying levels or degrees of assumptions. Because of an occasional need for comparison between the noise sensitivities among the particular cases considered, the formulation of the equations for all three cases is presented and then following is a consideration of noise effects on the estimates of these cases.

Case 1:  The General $Z_{xy}$ Equations

Of the six expressions which combine the various power

density spectra to result in the estimates of $Z_{xy}$, two tend to be

unstable for the noise-free, one dimensional situation (Sims, 1971).

The remaining four estimates are

$$Z_{xy} = \frac{\langle H_x E_y^* \rangle \langle E_x E_x^* \rangle - \langle H_x E_x^* \rangle \langle E_x E_y^* \rangle}{\langle H_x E_y^* \rangle \langle H_y E_x^* \rangle - \langle H_x E_x^* \rangle \langle H_y E_y^* \rangle} \qquad (3-1)$$

$$Z_{xy} = \frac{\langle H_x H_x^* \rangle \langle E_x E_x^* \rangle - \langle H_x E_x^* \rangle \langle E_x H_x^* \rangle}{\langle H_x H_x^* \rangle \langle H_y E_x^* \rangle - \langle H_x E_x^* \rangle \langle H_y H_x^* \rangle} \qquad (3-2)$$

$$Z_{xy} = \frac{\langle H_x E_y^* \rangle \langle E_x H_y^* \rangle - \langle H_x H_y^* \rangle \langle E_x E_y^* \rangle}{\langle H_x E_y^* \rangle \langle H_y H_y^* \rangle - \langle H_x H_y^* \rangle \langle H_y E_y^* \rangle} \qquad (3-3)$$

$$Z_{xy} = \frac{\langle H_x H_x^* \rangle \langle E_x H_y^* \rangle - \langle H_x H_y^* \rangle \langle E_x H_x^* \rangle}{\langle H_x H_x^* \rangle \langle H_y H_y^* \rangle - \langle H_x H_y^* \rangle \langle H_y H_x^* \rangle} \qquad (3-4)$$

In these four equations and those to follow in this section the

symbols $\langle\ \rangle$ denote the expected value of the auto or cross spectra

which they enclose while the symbol * indicates the complex

conjugate of the individual spectrum.

From this point on in this discussion an assumption is made

with regard to the type of noise encountered during the data

acquisition process.  Much of the noise introduced into the MT

data originates in the electronic circuits of the system.  Noise on

the MT results can also be created at the electric or magnetic field

sensors. For example, electrochemical changes at the E-field electrodes can introduce a wide frequency spectrum of noise into the data. These types of noise are generally incoherent between any two E and/or H channels.

It must be noted that, in some cases, coherency can exist in the noise between channels. As an example, unwanted coherent signals can be created on the electric field data from current transients on power lines when MT measurements are made in the vicinity of such lines. Nevertheless, observation has indicated that noise is incoherent among the channels in most instances. It is therefore assumed that any noise encountered is incoherent between any two of the MT data channels. This assumption is made for all cases considered here.

Equations (3-1) through (3-4) are the general expressions for the estimates of $Z_{xy}$ but may be simplified if certain assumptions are made as follows.

Case 2: Unpolarized Magnetic Field

A high degree of polarization of the source magnetic field presents some severe problems for the tensor MT method. Each of the impedance estimates given by Equations (3-1) through (3-4) is in essence an analytic solution of a pair of equations from a set of four containing the unknowns $Z_{xx}$ and $Z_{xy}$ (Sims, 1971), for

instance). If the magnetic field is strictly polarized, the orthogonal

components $H_x$ and $H_y$ are perfectly correlated (Spitznogle, 1966).

When this occurs, one or more pairs of the four equations from which

the impedance estimates are derived are no longer independent. The

general expressions for the impedance $Z_{xy}$ given previously are

therefore not valid. In general, the lower the coherency between

$H_x$ and $H_y$, the more reliable are the impedance estimates, all other

things being equal.

An additional assumption is therefore made for this and the

following case. For the purpose of this discussion the vector

magnetic field is assumed to be virtually unpolarized.

Experimental evidence has indicated that the measured

coherency between $H_x$ and $H_y$ is relatively low in many instances.

This is observed particularly throughout the lower portion of the

frequency spectrum where the source fields originate at the earth's

magnetosphere. It should be pointed out, however, that this

unpolarized feature is sometimes only approximately true and

occasionally may not be observed for some real conditions.

Specifically, the upper portion of the MT frequency spectrum may

present some problems related to the validity of unpolarized

magnetic field. The source for this part of the MT and AMT spectrum

originates from electrical discharges of atmospheric thunderstorms.

In some instances the energy from a local condition coupled with a lack of energy from more generally distributed sources may result in a polarization of the magnetic field.

For incoherent random noise and essentially unpolarized magnetic field, the expected or average value $\langle H_x H_y^* \rangle$ is comparatively small. The four estimates of $Z_{xy}$ for this case become

$$Z_{xy} = \frac{\langle H_x E_y^* \rangle \langle E_x E_x^* \rangle - \langle H_x E_x^* \rangle \langle E_x E_y^* \rangle}{\langle H_x E_y^* \rangle \langle H_y E_x^* \rangle - \langle H_x E_x^* \rangle \langle H_y E_y^* \rangle} \tag{3-5}$$

$$Z_{xy} = \frac{\langle H_x H_x^* \rangle \langle E_x E_x^* \rangle - \langle H_x E_x^* \rangle \langle E_x H_x^* \rangle}{\langle H_x H_x^* \rangle \langle H_y E_x^* \rangle} \tag{3-6}$$

$$Z_{xy} = \frac{\langle H_x E_y^* \rangle \langle E_x H_y^* \rangle}{\langle H_x E_y^* \rangle \langle H_y H_y^* \rangle} = \frac{\langle E_x H_y^* \rangle}{\langle H_y H_y^* \rangle} \tag{3-7}$$

$$Z_{xy} = \frac{\langle H_x H_x^* \rangle \langle E_x H_y^* \rangle}{\langle H_x H_x^* \rangle \langle H_y H_y^* \rangle} = \frac{\langle E_x H_y^* \rangle}{\langle H_y H_y^* \rangle} \tag{3-8}$$

Case 3: One or Two Dimensional Earth Models

If, in addition to incoherent noise and an unpolarized magnetic field, the earth's structure approaches a one dimensional case, the expressions (3-5) through (3-8) for $Z_{xy}$ may be further simplified. This is also possible for two dimensional situations if the data have been rotated to the principal axes as described in Chapter 2.

For these cases the non-orthogonal cross power terms such as $\langle E_x H_x^* \rangle$ are small in magnitude with respect to auto power terms and to orthogonal E-H pairs such as $\langle E_x H_y^* \rangle$. The first two estimates of Equations (3-5) and (3-6) are then approximately reduced to

$$Z_{xy} = \frac{\langle E_x E_x^* \rangle}{\langle H_y E_x^* \rangle} \qquad (3-9)$$

while the last two of Equations (3-7) and (3-8) are

$$Z_{xy} = \frac{\langle E_x H_y^* \rangle}{\langle H_y H_y^* \rangle} \, . \qquad (3-10)$$

The effects of incoherent noise on the estimates of $Z_{xy}$ are most easily determined for a one dimensional earth with unpolarized magnetic field. Let the spectra needed for the estimates given in Equations (3-9) and (3-10) be

$$E_x = E_{xs} + E_{xn} \qquad (3-11)$$

$$E_y = E_{ys} + E_{yn} \qquad (3-12)$$

$$H_y = H_{ys} + H_{yn} \qquad (3-13)$$

where $E_{xs}$, $E_{ys}$ and $H_{ys}$ represent the true signal portion of the spectra, and $E_{xn}$, $E_{yn}$, and $H_{yn}$ are the random noise components of the spectra. If it is assumed that the noise is incoherent between channels and independent of signal, then terms such as $\langle E_{xs} E_{xn}^* \rangle$

and $\langle H_{yn} E^*_{xn} \rangle$ are zero so that the estimate of $Z_{xy}$ for the one dimensional case given by Equation (3-9) becomes

$$Z_{xy} = \frac{\langle E_{xs} E^*_{xs} \rangle + \langle E_{xn} E^*_{xn} \rangle}{\langle H_{ys} E^*_{xs} \rangle} \qquad (3-14)$$

while the estimate of Equation (3-10) is

$$Z_{xy} = \frac{\langle E_{xs} H^*_{ys} \rangle}{\langle H_{ys} H^*_{ys} \rangle + \langle H_{yn} H^*_{yn} \rangle} \cdot \qquad (3-15)$$

It can be seen that the magnitude of $Z_{xy}$ of the first expression is biased upward from its true value by random noise on $E_x$ while the magnitude of the second estimate in Equation (3-17) decreases in value when noise is present on $H_y$ (Sims, et. al., 1971).

The numerator of Equation (3-14) is a real quantity as is the denominator of Equation (3-15). The phase of the first estimate is thus determined by the complex denominator while that of the second is given by the complex numerator. In each instance the complex quantities which determine the phase contain no noise terms, so that the phase of $Z_{xy}$ in Equations (3-14) and (3-15) is unaffected by random noise on $E_x$ and $H_y$. Therefore, for unpolarized magnetic field and a one dimensional earth, the magnitude of every estimate of $Z_{xy}$ is biased in some way by noisy data whereas the phase of each retains its true value. The phase information is thus of considerable importance for this case.

For the second case under consideration when the magnetic field is unpolarized, the effect of incoherent noise on the magnitudes and phases of the estimates given by (3-7) and (3-8) are the same as for the corresponding estimates in the one dimensional case. Thus, for these two estimates, the magnitudes are biased by noise while the phases are unbiased.

The estimate for Case 2 given by Equation (3-6) contains auto power terms of both $E_x$ and $H_y$. As noise increases on both of these channels, the magnitude of this estimate is more strongly influenced by noise on $E_x$ and is biased upward in this case. Since

$$\langle H_x E_x^* \rangle \langle E_x H_x^* \rangle = |H_x E_x^*|^2 \qquad (3-16)$$

the numerator of the second estimate of this set is real and thus the phase of this estimate is solely determined by the term $\langle H_y E_x^* \rangle$. It can then be seen that the phase of (3-6) is not biased by incoherent noise on the E and H data.

Since the only auto spectra term present in Equation (3-5) is $\langle E_x E_x^* \rangle$, the magnitude of this estimate is biased upward by random noise on $E_x$. But, because this auto spectra quantity exists in the complex numerator of this estimate, no specific statement can be made as to how noise effects the phase of this estimate. As the form of this estimate was not simplified through the assumptions made for this case, it is identical to the same estimate of the general

case. Some general observations will be developed for this estimate during the discussion of Case 1.

It can therefore be seen that for an unpolarized magnetic field the amplitudes of all four estimates under consideration are biased by noise on $E_x$ and $H_y$. However, the phases of three of these estimates are unaffected by random noise. For this case, then, the phase is a valuable function if the amplitude can be derived from it.

Returning to the general case as given by Equations (3-1) through (3-4), we may make comments about the effects of noise on these estimates. It might be informative to examine the manner in which extreme amounts of noise affect the amplitude and phase of these expressions. As incoherent noise increases on the electric or magnetic field channels, products involving auto power terms become dominant over other products of the equations. It can then be seen that, in this case, the estimates given by (3-2) and (3-4) approach the one dimensional estimate of (3-9). Although the amplitudes of these two estimates are severely corrupted by a large amount of noise, the phase of each theoretically limits to that of $E_x H_y^*$.

It is also interesting to note that, regardless of the level of incoherent noise on E or H, the phases of the estimates given by (3-2) and (3-4) are identically equal whereas the amplitudes diverge as noise increases. This, coupled with the observation that both phases tend toward the one dimensional case for large amounts of incoherent noise, might well indicate a priority use of these two estimates if the phase information is considered valuable.

It is thus evident that in some cases the magnitudes and phases of the various MT impedance estimates behave differently with respect to random noise. One may sometimes intuitively feel that, as more and more data are accumulated at a specific frequency, the effects of noise will eventually average out. Such is not the case for the amplitude of the tensor impedance (or admittance) estimates. The auto power density spectra for channels on which noise is present do not ultimately converge to their noise-free values. The estimates containing these terms are therefore biased by noise. As has been seen, however, the phases of some of the $Z_{xy}$ estimates in some instances do converge to their noise-free values if sufficient data are available.

As is shown in a subsequent chapter, it is possible under certain assumptions to derive the apparent resistivity function primarily from the phase of Z. From Equations (2-7) and (2-8) the

apparent resistivities as derived from the magnitude of Z involves

squaring $|Z|$. This process accentuates any inaccuracies of $|Z|$ due

to noise and thus results in even more scatter on $\rho_A$. If the conditions

are such that the phase is less biased than is $|Z|$, and if $\rho_A$ can be

derived from it, then the value of the phase information becomes

apparent.

### B. Measurement Statistics

In the preceding discussion it was assumed that an unlimited

amount of data was acquired so that the measured or estimated

values of $|Z|$ and $\varphi$ converged to their biased or unbiased expected

values. Such is not the case for practical MT surveys, however.

The accumulation of a large number of independent samples at the

lower frequencies requires a great amount of data acquisition time.

The length of time for which each MT site is occupied becomes an

important consideration for these surveys if measurements at a number

of sites are to be made.

The following discussion is given to illustrate the effects of a

limited number of data samples upon the measured values of the appar-

ent resistivity ($\rho_{Am}$) and the phase of impedance ($\varphi_m$) in the presence

of noise. From Equation (2-7) the estimated apparent resistivity is

$$\rho_{Am} = \frac{1}{\omega\mu} |Z_m|^2 . \qquad (3-17)$$

The statistical variances of $\rho_{Am}$ and $\varphi_m$ about their expected values are determined not only as a function of the noise levels present, but also in terms of the number of independent samples obtained. For the purpose of this study a strictly one dimensional earth is assumed so that the scalar (or Cagniard) impedance

$$Z = Z_{xy} = \frac{E_x}{H_y} \qquad (3-18)$$

is representative of the earth's impedance. From this point on the x and y subscripts will be omitted. It is understood that these two field components are orthogonal.

Let the sampled field quantities be given as

$$E_m = E + E_n \qquad (3-19)$$

and

$$H_m = H + H_n \qquad (3-20)$$

where E and H represent the true values of each sample while $E_n$ and $H_n$ are the noise components of the sample. The expected values of the auto power spectra terms are defined by

$$E\{EE^*\} = P_E \qquad (3-21)$$

$$E\{HH^*\} = P_H \qquad (3-22)$$

$$E\{E_n E_n^*\} = P_{En} \tag{3-23}$$

$$E\{H_n H_n^*\} = P_{Hn} \tag{3-24}$$

In this discussion $E\{\ \}$ designates the expected value of the quantity enclosed by the braces. Since noise is assumed to be incoherent between channels and independent of signal, the expected values of the cross power terms involving noise spectra are zero so that

$$E\{EH_n^*\} = E\{HE_n^*\} = E\{E_n H_n^*\} = 0 \tag{3-25}$$

and

$$E\{EE_n^*\} = E\{HH_n^*\} = 0 \quad . \tag{3-26}$$

One measure of the degree of noise present on the data is the coherency between the measured E and H field spectra. This parameter may be defined as

$$C = \frac{|E\{E_m H_m^*\}|}{\sqrt{E\{E_m E_m^*\} E\{H_m H_m^*\}}} \quad . \tag{3-27}$$

From the definitions of Equations (3-19) and (3-20),

$$E\{E_m H_m^*\} = E\{EH^*\} + E\{EH_n^*\} + E\{E_n H^*\} + E\{E_n H_n^*\} \tag{3-28}$$

which, with Equations (3-25) and (3-26), becomes

$$E\{E_m H_m^*\} = E\{EH^*\} \quad . \tag{3-29}$$

But the actual impedance Z is defined by

$$E = ZH. \tag{3-30}$$

When Equations (3-22), (3-29) and (3-30) are combined, it is found that

$$\left| E\{E_m H_m^*\} \right| = |Z| P_H. \tag{3-31}$$

In a similar manner it can be shown that

$$E\{E_m E_m^*\} = P_E + P_{En} \tag{3-32}$$

and

$$E\{H_m H_m^*\} = P_H + P_{Hn} \tag{3-33}$$

so that the coherency is given in terms of the signal and noise power of $E_m$ and $H_m$ as

$$C = \frac{|Z| P_H}{\sqrt{(P_E + P_{En})(P_H + P_{Hn})}}. \tag{3-34}$$

Since

$$|Z|^2 = \frac{E\{EE^*\}}{E\{HH^*\}} = \frac{P_E}{P_H} \tag{3-35}$$

the coherency function is then defined as

$$C = \frac{1}{\sqrt{\left(1 + \dfrac{P_{En}}{P_E}\right)\left(1 + \dfrac{P_{Hn}}{P_H}\right)}}. \tag{3-36}$$

It can be seen that the coherence has a value of unity for no noise on the E and H channels. As noise increases on either E or H (or both), C decreases in value and approaches zero for the completely noisy situation. If both of the electric and magnetic field channels are noisy to an extent that the measured spectra are combinations of equal noise and signal power, the coherency is 0.5. On the other hand if noise exists on only one of the channels, an equal amount of noise power and signal power on the noisy channel results in a coherency value of about 0.7.

For a one dimensional earth model considered in this discussion the measured apparent resistivity can be expressed as

$$\rho_{Am} = \frac{1}{\omega\mu} \frac{\langle |E_m|^2 \rangle}{\langle |H_m|^2 \rangle} \tag{3-37}$$

where the symbols $\langle \ \rangle$ indicate an average of M independent samples. Equation (3-37) may be rewritten as

$$\rho_{Am} = \frac{1}{\omega\mu} \frac{\langle E_m E_m^* \rangle}{\langle H_m H_m^* \rangle} . \tag{3-38}$$

Noise on either the E or the H channels affects the estimation of $\rho_{Am}$. First consider the case of E noise only.

In this case

$$\rho_{Am} = \frac{\langle (E + E_n) (E* + E_n*) \rangle}{\omega \mu \langle HH* \rangle}$$  (3-39)

which is

$$\rho_{Am} = \frac{\langle EE* \rangle + 2 \operatorname{Re} \langle EE_n* \rangle + \langle E_n E_n* \rangle}{\omega \mu \langle HH* \rangle}$$  (3-40)

where Re ( ) means the "real part of". The ratio between the
noiseless auto power averages of E and H is

$$|Z|^2 = \frac{\langle EE* \rangle}{\langle HH* \rangle}$$  (3-41)

so that Equation (3-40) may be expressed as

$$\frac{\rho_{Am}}{\rho_A} = 1 + \frac{2 \operatorname{Re} \langle EE_n* \rangle + \langle E_n E_n* \rangle}{|Z|^2 \langle HH* \rangle} .$$  (3-42)

The variation of the estimated apparent resistivity about its expected
value may be expressed as the statistical variance of Equation (3-42).
This is defined as

$$\sigma_{\rho_A}^2 = V \left\{ \frac{\rho_{Am}}{\rho_A} \right\} = V \left\{ \frac{2 \operatorname{Re} \langle EE_n* \rangle + \langle E_n E_n* \rangle}{|Z|^2 \langle HH* \rangle} \right\}$$  (3-43)

where $V \{ \}$ is the standard definition of the variance.

At this point it is assumed that the average $\langle HH* \rangle$ is very
nearly equal to $P_H$ as in Equation (3-22) and that the term $\operatorname{Re} \langle EE_n* \rangle$
dominates the variance given by Equation (3-43) so that for

averages consisting of M samples,

$$\sigma^2_{\rho_A} \simeq \frac{4}{MP^2_H |Z|^4} V\{Re(EE^*_n)\} .$$  (3-44)

But

$$Re(EE^*_n) = Re(E) Re(E_n) + Im(E) Im(E_n)$$  (3-45)

where $Im(\ )$ denotes the imaginary part of the complex quantity within the parentheses. If the real and imaginary parts of $E$ and $E_n$ are independent random variables with zero means,

$$V\{Re(EE^*_n)\} = E\{Re^2(E)\} E\{Re^2(E_n)\}$$

$$+ E\{Im^2(E)\} E\{Im^2(E_n)\}$$  (3-46)

where again $E\{\ \}$ means the expected value of the enclosed random variable. If $Re(E)$ and $Im(E)$ are independent random variables having the same statistics, and since

$$E\{Re^2(E) + Im^2(E)\} = P_E$$  (3-47)

then

$$E\{Re^2(E)\} = E\{Im^2(E)\} = \frac{P_E}{2}$$  (3-48)

and also

$$E\{Re^2(E_n)\} = E\{Im^2(E_n)\} = \frac{P_{En}}{2} .$$  (3-49)

The combination of Equations (3-35), (3-44), (3-46), (3-48) and (3-49) results in the variance of the apparent resistivity error as a function of the E field signal and noise power as

$$\sigma^2_{\rho_A} \simeq \frac{2P_{En}}{M\,P_E} \; . \tag{3-50}$$

For noise only on the E channel the coherency as defined by Equation (3-36) combined with Equation (3-50) results in

$$\sigma^2_{\rho_A} \simeq \frac{2}{M} \left( \frac{1}{C^2} - 1 \right) \; . \tag{3-51}$$

For noise on the magnetic field channel a development similar to the one given above may be used to determine the statistical variance in the $\rho_A$ estimation. For noise present on the H data the measured apparent resistivity is

$$\rho_{Am} = \frac{\langle EE* \rangle}{\langle (H + H_n)(H* + H_n^*) \rangle} \tag{3-52}$$

which may be written as

$$\frac{\rho_{Am}}{\rho_A} = \frac{1}{1 + \dfrac{N_H}{\langle HH* \rangle}} \tag{3-53}$$

where

$$N_H = 2 \, \mathrm{Re} \langle HH_n^* \rangle + \langle H_n H_n^* \rangle \; . \tag{3-54}$$

If the first terms of a power series expansion of Equation (3-53) are
assumed to be the major contribution to the series, then

$$\frac{\rho_{Am}}{\rho_A} \simeq 1 - \frac{N_H}{\langle HH^* \rangle} \quad . \tag{3-55}$$

If the variance of this equation is determined in the same manner as
that for the E noise case given previously, one finds that $\sigma_{\rho_A}^2$ is the
same as that given by Equation (3-51). The standard deviation (or
variance) of the error involved in the apparent resistivity measure-
ment is affected not only by the noise level encountered but also by
the number of independent samples accumulated in the measurements.
This result is shown graphically in the upper portion of Figure 3-1.

A method similar to that outlined above may be used to yield
the approximate standard deviation of the error involved in the
measured MT phase information. Let this phase for a one dimensional
earth be defined as

$$\varphi_m = \tan^{-1} \left[ \frac{Im \langle E_m H_m^* \rangle}{Re \langle E_m H_m^* \rangle} \right] . \tag{3-56}$$

Utilizing the definitions of Equations (3-19) and (3-20) in Equation
(3-56) and expanding the resulting expression for $\varphi_m$ about

$$\varphi = \tan^{-1} \left[ \frac{Im(Z)}{Re(Z)} \right] . \tag{3-57}$$
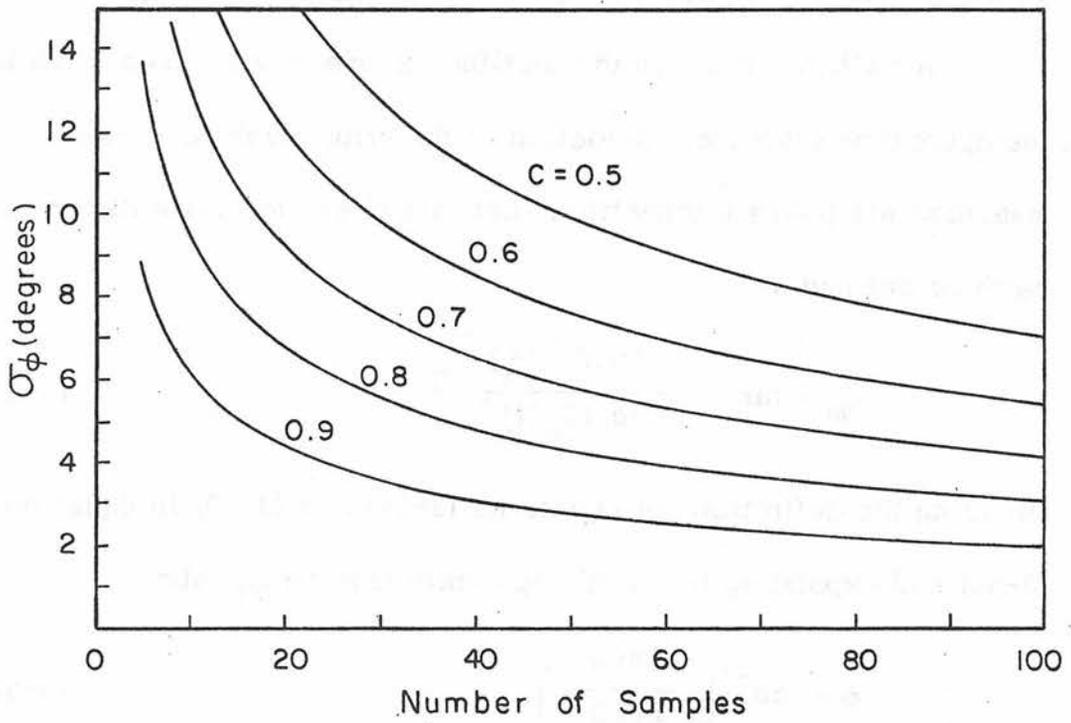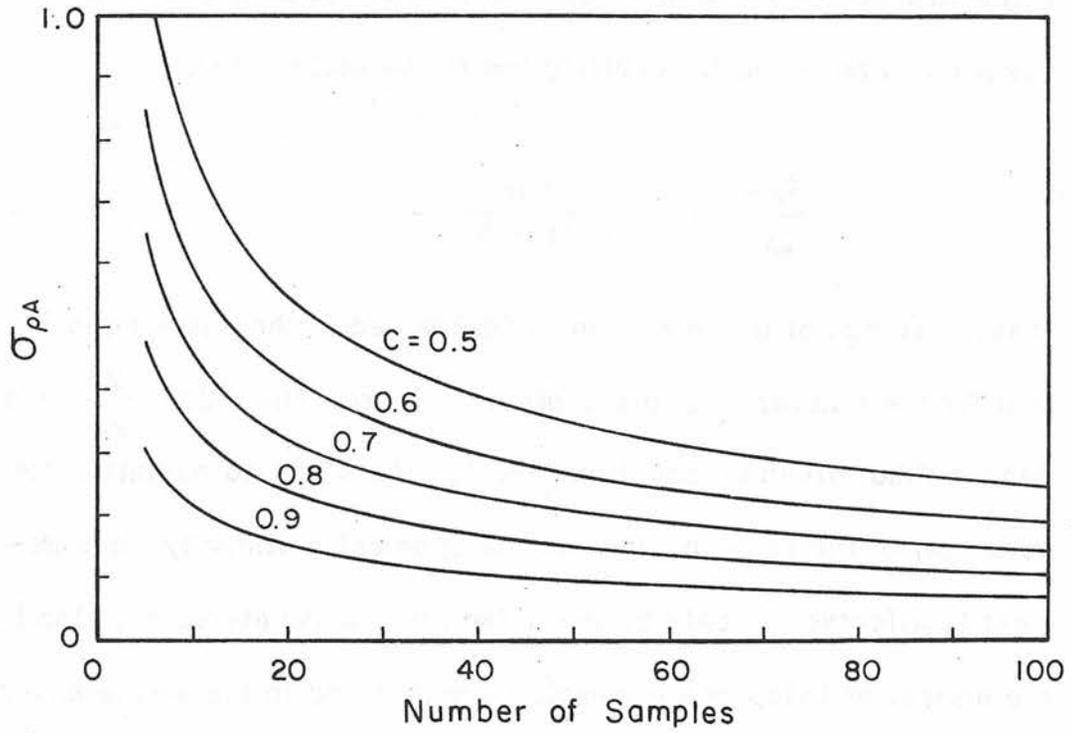
Fig. 3-1. STANDARD DEVIATION OF $\rho_A$ AND $\phi$ MEASUREMENTS

One may ultimately derive the standard deviation of the measured

phase error as

$$\sigma_{\varphi m} = \sqrt{\frac{1}{2M} \left(\frac{1}{C^2} - 1\right)} \qquad (3-58)$$

where as before M is the number of independent samples obtained,

C is the coherency measure of the data as defined by Equation (3-36),

and the standard deviation formula for the phase has units of

radians. The results of Equation (3-58) are plotted in Figure 3-1.

It can be seen from the curves of Figure 3-1 that the data

coherency must be high if the standard deviation of measured $\rho_A$ and

$\varphi$ is to be kept small for a reasonable number of sample points. This

is particularly true at the lowest frequencies of the MT data as few

independent samples are available without a lengthy occupation of

the MT sites.

The phase smoothing procedure outlined here does not

completely eliminate the need for $|Z|$ data. It is important that

any noise effects present on the amplitude function be minimized.

The corruption of $|Z|$ due to noise can be reduced in several ways.

Some obvious methods present themselves when an examination of

the various estimates is made. The choice of estimates used in the

MT analysis should depend upon the particular situation encountered.

For instance, it is sometimes evident that a greater proportion of

noise is present on either the E data or the H data in some range of the frequency spectrum. In this case it is obviously desirable to utilize only a single estimate which is insensitive to this noise. At other times field tests may indicate noise on all channels at some frequencies, and so a geometric mean of the various biased estimates may be used.

One method which may be used to estimate the noise levels encountered in the MT measurement process is to run a parallel sensor test. This is done by aligning both the $H_x$ and $H_y$ magnetometers parallel to each other and arranging the electrode pairs of $E_x$ and $E_y$ in a parallel fashion. For the noise-free case the outputs of the two E field MT channels should be identical as should the H field outputs. If these parallel measurements are made throughout the MT frequency spectrum and coherencies are computed for the two E channels and for the two H channels, one can determine which channels contain noise. Thus a decision may be made regarding the selection of estimate or estimates based on these noise measurements.

## IV. THE PHASE SMOOTHING EQUATIONS

Many of the situations encountered in MT prospecting involve
data which is one or two dimensional in nature. In these situations
it is the common current practice to utilize the one dimensional
inversion techniques as indicated in Chapter 2. When three
dimensional data are encountered, however, little can be done other
than performing a best fit one dimensional model to the data. In
other words, regardless of the actual subsurface structure, the normal
practice is to use the various inversion methods to derive a layered
model for the MT sites.

It can be shown that the surface MT tensor impedance of a
horizontally stratified earth with homogeneous layers is a minimum
phase function (Kunetz, 1972). This means that the complex transfer
function $Z(\omega)$ contains no poles or zeros in the right half of the
complex plane. The purpose of this section is to utilize the minimum
phase property in the development of formulas which are useful in
the MT data analysis procedure. The application of these relations
are referred to as the "phase smoothing" process.

For the sake of completeness the development of the phase
smoothing equations will begin with the Hilbert Transform pair. For
a discussion of this transform and some of the following expressions

see Bode (1945), Guillemin (1951), Oppenheim and Schafer (1975), and others.

If the complex variable $Z(\omega)$ represents a real, causal system, it has no poles in the right half of the complex plane. The real and imaginary parts defined as

$$Z(\omega) = R(\omega) + jQ(\omega) \tag{4-1}$$

are related through the Hilbert Transform pair at radian frequency $\omega_o$ by

$$R(\omega_o) = \frac{1}{\pi} \int_{-\infty}^{\infty} \frac{Q(\omega)}{\omega_o - \omega} \, d\omega \tag{4-2}$$

and

$$Q(\omega_o) = -\frac{1}{\pi} \int_{-\infty}^{\infty} \frac{R(\omega)}{\omega_o - \omega} \, d\omega \, . \tag{4-3}$$

An alternate way of expressing the complex $Z(\omega)$ is in amplitude/ phase form as

$$Z(\omega) = |Z(\omega)| e^{j\varphi} \, . \tag{4-4}$$

Now consider the complex variable given by the natural logarithm of $Z(\omega)$

$$\ln Z(\omega) = \ln |Z(\omega)| + j\varphi(\omega) \, . \tag{4-5}$$

If the Hilbert Transform pair is to be applied to the real and imaginary parts of $\ln Z(\omega)$, then this variable must represent a real, causal system. In other words it must be analytic in the right half of the complex plane. Since both the poles and zeros of $Z(\omega)$ become the poles $\ln Z(\omega)$, the requirement of causality for $\ln Z(\omega)$ is equivalent to $Z(\omega)$ not having any poles or zeros in the right half plane. Thus, if the Hilbert Transform is to be applied to $\ln Z(\omega)$, the complex variable $Z(\omega)$ must be a minimum phase function. In this case

$$\ln |Z(\omega_o)| = \frac{1}{\pi} \int_{-\infty}^{\infty} \frac{\varphi(\omega)}{\omega_o - \omega} \, d\omega \tag{4-6}$$

and

$$\varphi(\omega_o) = -\frac{1}{\pi} \int_{-\infty}^{\infty} \frac{\ln |Z(\omega)|}{\omega_o - \omega} \, d\omega. \tag{4-7}$$

Any function $f(x)$ may be expressed as the sum of an even function and odd function of $x$ as

$$f(x) = f_e(x) + f_o(x) \tag{4-8}$$

where

$$f_e(x) = \frac{1}{2} [f(x) + f(-x)] \tag{4-9}$$

and

$$f_o(x) = \frac{1}{2}[f(x) - f(x)].$$ (4-10)

Applying Equations (4-8) through (4-10) to the integrand of Equation (4-7) gives

$$\varphi(\omega_o) = -\frac{1}{2\pi}\int_{-\infty}^{\infty}\left[\frac{\ln|Z(\omega)|}{\omega_o - \omega} + \frac{\ln|Z(-\omega)|}{\omega_o + \omega}\right]d\omega$$

(4-11)

$$-\frac{1}{2\pi}\int_{-\infty}^{\infty}\left[\frac{\ln|Z(\omega)|}{\omega_o - \omega} - \frac{\ln|Z(-\omega)|}{\omega_o + \omega}\right]d\omega$$

where the expression enclosed by the brackets in the first integral is an even function of $\omega$ and the term in the brackets of the second integral is an odd function of $\omega$.

Since the integral of an odd function of $\omega$ throughout the range $-\infty \leq \omega \leq \infty$ is identically zero, the second integral of Equation (4-11) vanishes, resulting in

$$\varphi(\omega_o) = -\frac{1}{2\pi}\int_{-\infty}^{\infty}\left[\frac{\ln|Z(\omega)|}{\omega_o - \omega} + \frac{\ln|Z(-\omega)|}{\omega_o + \omega}\right]d\omega.$$ (4-12)

Noting that the limits of integration may be changed to $o \leq \omega \leq \infty$ for integration of the even function of $\omega$ given by Equation (4-12) and rearranging the integrand of this expression gives

$$\varphi(\omega_o) = -\frac{1}{\pi}\int_{0}^{\infty}\frac{(\omega_o + \omega)\ln|Z(\omega)| + (\omega_o - \omega)\ln|Z(-\omega)|}{\omega_o^2 - \omega^2}d\omega$$ (4-13)

or

$$\varphi(\omega_0) = -\frac{1}{\pi} \int_0^\infty \left\{ \omega_0 \frac{[\ln |Z(\omega)| + \ln |Z(-\omega)|]}{\omega_0^2 - \omega^2} \right. \tag{4-14}$$

$$\left. + \frac{\omega [\ln |Z(\omega)| - \ln |Z(-\omega)|]}{\omega_0^2 - \omega^2} \right\} d\omega .$$

If $\ln Z(\omega)$ is to be physically realizable, then

$$\ln |Z(\omega)| = \ln |Z(-\omega)| \tag{4-15}$$

so that Equation (4-14) becomes

$$\varphi(\omega_0) = -\frac{2}{\pi} \int_0^\infty \frac{\omega_0 \ln |Z(\omega)|}{\omega_0^2 - \omega^2} d\omega . \tag{4-16}$$

The form of this expression may be modified as

$$\varphi(\omega_0) = \frac{1}{\pi} \int_0^\infty \frac{\ln |Z(\omega)|}{\frac{1}{2}\left(\frac{\omega}{\omega_0} - \frac{\omega_0}{\omega}\right)} \frac{d\omega}{\omega} . \tag{4-17}$$

If a change of variables is used such that

$$\frac{\omega}{\omega_0} = e^u \tag{4-18a}$$

or

$$u = \ln \omega - \ln \omega_0 \tag{4-18b}$$

and

$$du = d(\ln \omega) = \frac{d\omega}{\omega} . \tag{4-19}$$

Equation (4-17) then becomes

$$\varphi(\omega_o) = \frac{1}{\pi} \int_{-\infty}^{\infty} \frac{\ln |Z(\omega)|}{\frac{1}{2}(e^u - e^{-u})} \, du \qquad (4\text{-}20)$$

or

$$\varphi(\omega_o) = \frac{1}{\pi} \int_{-\infty}^{\infty} \frac{\ln |Z(\omega)|}{\sinh(u)} \, du \, . \qquad (4\text{-}21)$$

Equation (4-21) may now be integrated by parts. In the formula for integration by parts

$$\int p \, dq = pq - \int q \, dp \qquad (4\text{-}22)$$

let

$$p = \ln |Z(\omega)|, \; dp = \frac{d(\ln |Z(\omega)|)}{du} \, du \qquad (4\text{-}23a)$$

then

$$dq = \frac{du}{\sinh(u)} \, , \; q = \ln \tanh\left(\frac{|u|}{2}\right) = -\ln \coth \frac{|u|}{2} \, . \qquad (4\text{-}23b)$$

When Equation (4-21) is integrated as in (4-22) with the definitions given by Equations (4-23), the result is

$$\varphi(\omega_o) = \frac{1}{\pi} \ln |Z(\omega)| \ln \tanh\left(\frac{|u|}{2}\right) \Big|_{-\infty}^{\infty}$$
$$+ \frac{1}{\pi} \int_{-\infty}^{\infty} \frac{d(\ln |Z(\omega)|)}{du} \ln \coth\left(\frac{|u|}{2}\right) du. \qquad (4\text{-}24)$$

The ln tanh function vanishes at both limits. Although $|Z(\omega)|$ may approach zero at one or both of the limits, the manner in which

$\ln |Z(\omega)|$ increases in value is such that the ln tanh term dominates. The first term of Equation (4-24) therefore vanishes. The phase of a minimum phase function is thus related to the amplitude at radian frequency $\omega_o$ by

$$\varphi(\omega_o) = \frac{1}{\pi} \int_{-\infty}^{\infty} \frac{d(\ln |Z(\omega)|}{du} \ln \coth \left( \frac{|u|}{2} \right) du. \qquad (4\text{-}25)$$

In order to simplify the notation of the following equations, let

$$y = \ln \omega, \quad y_o = \ln \omega_o \qquad (4\text{-}26a)$$

$$u = y - y_o \qquad (4\text{-}26b)$$

$$s(y) = \frac{d(\ln |Z(\omega)|)}{d(\ln \omega)} \qquad (4\text{-}27)$$

and

$$f(y_o - y) = \ln \coth \left( \frac{|y - y_o|}{2} \right). \qquad (4\text{-}28)$$

If $Z(\omega)$ represents the MT impedance, then $s(y)$ is the slope of the magnitude of this function on a natural log scale of $|Z|$ vs. $\omega$. With the notation given above, Equation (4-25) is written as

$$\varphi(y_o) = \frac{1}{\pi} \int_{-\infty}^{\infty} s(y) \, f(y_o - y) dy. \qquad (4\text{-}29)$$

The phase of $Z(\omega)$ is thus given by the convolution of the derivative or slope of $\ln |Z|$ with $f(y)$ where both are functions of $\ln \omega$. The Fourier transform of this convolution is

$$\Phi(x) = \frac{1}{\pi} S(x) F(x) \qquad (4\text{-}30)$$

where $\Phi(x)$, $S(x)$ and $F(x)$ represent the Fourier transforms of $\varphi(y)$,

$s(y)$ and $f(y)$, respectively. The variable $s(y)$ may then be expressed

as

$$s(y) = \pi \, \mathcal{F}^{-1} \left\{ \frac{\Phi(x)}{F(x)} \right\} \qquad (4\text{-}31)$$

where $\mathcal{F}^{-1}\{\ \}$ denotes the inverse Fourier transform of the quantity

within the braces. It can be shown that the Fourier transform of $f(y)$

defined by Equation (4-28) is

$$F(x) = \frac{\pi^2}{2} \; \frac{\tanh\left(\frac{\pi x}{2}\right)}{\left(\frac{\pi x}{2}\right)} \qquad (4\text{-}32)$$

If the integral suggested by Equation (4-27) is evaluated,

then the impedance magnitude $|Z|$ is derived entirely from the phase

of Z (less a constant of integration which will be considered later).

One means of evaluating Equation (4-31) for real data would

involve the utilization of interpolation and Fast Fourier transform (FFT)

routines on a digital computer. An approximation was desired by

this laboratory for $s(y)$ which could be evaluated even with small

computing devices such as a handheld calculator. For this reason

an alternate expression for $s(y)$ is developed which gives $s(y)$ as

a first order (or approximate) term and a second order (or correction) term.

Equation (4-29) may be written as

$$\varphi(y_0) = \frac{1}{\pi} s(y_0) \int\limits_{-\infty}^{\infty} f(y_0 - y)\, dy + \frac{1}{\pi} \int\limits_{-\infty}^{\infty} [s(y) - s(y_0)]\, f(y_0 - y)\, dy.$$

$$(4-33)$$

From a table of integrals (Dwight, 1964) it is found that

$$\int\limits_{-\infty}^{\infty} f(y_0 - y)\, dy = \int\limits_{-\infty}^{\infty} \ln \coth\left(\frac{|u|}{2}\right)\, du = \frac{\pi^2}{2} \qquad (4-34)$$

so that the expression for the phase of Equation (4-33) becomes

$$\varphi(y_0) = \frac{\pi}{2} s(y_0) + \frac{1}{\pi} \int\limits_{-\infty}^{\infty} [s(y) - s(y_0)]\, f(y_0 - y)\, dy \qquad (4-35)$$

or

$$s(y_0) = \frac{2}{\pi} \varphi(y_0) + \frac{2}{\pi^2} \int\limits_{-\infty}^{\infty} [s(y_0) - s(y)]\, f(y_0 - y)\, dy. \qquad (4-36)$$

The shape of the convolution function $f(y_0 - y)$ is shown in Figure 4-1. As can be seen from this figure, the value of $f(y_0 - y)$ decreases rapidly as the variable y diverges from the point $y_0$. Thus the major contribution of the integral portion of Equation (4-36) is determined in the vicinity of $y = y_0$. It is also noted that the function $s(y) - s(y_0)$ vanishes at the point $y = y_0$ where a singularity exists for $f(y_0 - y)$.
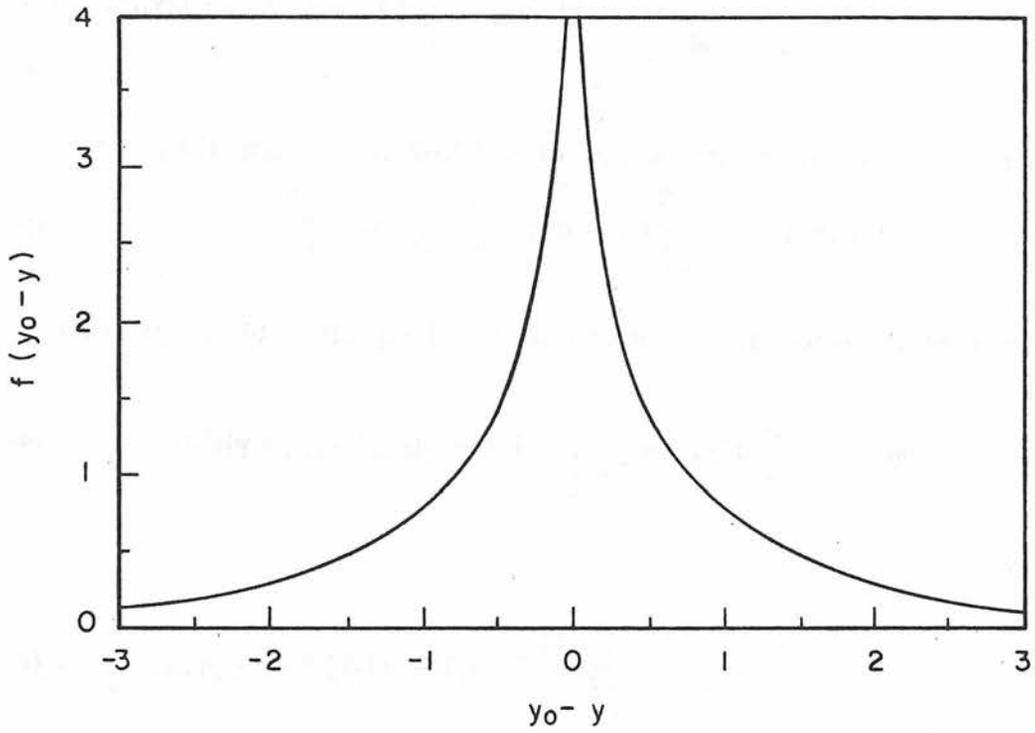
Fig. 4-1. CONVOLUTION FUNCTION

If the slope of $|Z(\omega)|$ vs. frequency on a log basis is constant or varies slowly enough primarily in the vicinity of $y = y_0$, the slope at this point is very nearly defined by

$$s(y_0) \simeq \frac{2}{\pi} \varphi(y_0).$$  (4-37)

In these situations the magnitude of the MT impedance function may be derived from the phase as

$$\ln |Z| \simeq \frac{2}{\pi} \int \varphi(y) dy + c$$  (4-38)

where c is a constant of integration to be considered later.

The situations encountered when applying the MT method are often such that $\ln |Z|$ does not vary slowly enough with respect to $\ln(\omega)$ to permit the use of the approximation given by Equation (4-38). In these cases the entire expression of Equation (4-36) must be utilized when deriving the amplitude of $Z(\omega)$ from its phase.

Let the second order term of Equation (4-36) be denoted as

$$\psi(y_0) = \frac{2}{\pi^2} \int_{-\infty}^{\infty} [s(y_0) - s(y)] f(y_0 - y) dy$$  (4-39)

or using Equation (4-34)

$$\psi(y_0) = s(y_0) - \frac{2}{\pi^2} [s(y_0) * f(y_0)]$$  (4-39a)

where the symbol (*) represents the convolution process. The Fourier Transform of this second order term is then

$$\Psi(x) = S(x) \left[ 1 - \frac{2}{\pi^2} F(x) \right] \tag{4-40}$$

where $\Psi(x)$ is the Fourier transform of $\psi(y)$, etc.

Equations (4-30) and (4-40) may be combined to give

$$\Psi(x) = \pi \Phi(x) \left[ \frac{1}{F(x)} - \frac{2}{\pi^2} \right]. \tag{4-41}$$

In the ln radian frequency domain the second order term is

$$\psi(y_0) = \pi \mathcal{F}^{-1} \left\{ \Phi(x) \left[ \frac{1}{F(x)} - \frac{2}{\pi^2} \right] \right\}. \tag{4-42}$$

The second order term of the derivative of $\ln |Z|$ with respect to $\ln(\omega)$ may finally be written using Equation (4-32) as

$$\psi(y_0) = \frac{2}{\pi} \mathcal{F}^{-1} \left\{ T(x) \Phi(x) \right\} \tag{4-43}$$

where the Fourier transform of the new convolver, $T(x)$, is defined as

$$T(x) = \frac{\frac{\pi x}{2}}{\tanh \frac{\pi x}{2}} - 1. \tag{4-44}$$

The derivative or slope of $\ln |Z|$ with respect to $\ln(\omega)$ may thus be expressed through the combination of Equations (4-27), (4-36), (4-39), and (4-43) as

$$\frac{d(\ln |Z|)}{d(\ln \omega)} = \frac{2}{\pi} \varphi(\ln \omega) + \frac{2}{\pi} \mathcal{F}^{-1} \left\{ T(x) \Phi(x) \right\} \tag{4-45}$$

which may in turn be integrated with respect to $\ln(\omega)$ to yield the phase derived MT impedance magnitude function as

$$\ln |Z(\omega)| = \frac{2}{\pi} \int \Phi(\ln \omega) \, d(\ln \omega) + \frac{2}{\pi} \int \mathcal{F}^{-1} \{T(x)\} \, d(\ln \omega) + c$$

(4-46)

where c is the constant of integration. This is the basic formula for the phase smoothing process but may be slightly modified for practical reasons.

During the MT analysis process it is often more convenient to think in terms of the apparent resistivity function $\rho_A$ rather than in terms of $|Z|$. The phase smoothing formula of Equation (4-46) may be defined for $\rho_A$ through a simple substitution of variables. Since the MT apparent resistivity is given by

$$\rho_A = \frac{1}{\omega\mu} |Z|^2$$

(4-47)

then

$$\ln \rho_A = 2 \ln |Z| - \ln \omega + \text{constant}$$

(4-48)

If the derivative of Equation (4-48) is taken with respect to the variable $\ln \omega$, then

$$\frac{d(\ln |Z|)}{d(\ln \omega)} = \frac{1}{2} \left[ \frac{d(\ln \rho_A)}{d(\ln \omega)} + 1 \right].$$

(4-49)

Substitution of Equation (4-49) into (4-45) yields

$$\frac{d(\ln \rho_A)}{d(\ln \omega)} = \left[ \frac{4}{\pi} \varphi(\ln \omega) - 1 \right] + \frac{4}{\pi} \mathcal{F}^{-1} \{T(x) \, \Phi(x)\} \quad (4-50)$$

where the expression within the brackets is the first order term and T(x) in the remaining term is defined as in Equation (4-44).

In order to provide the final formula for the phase smoothing process, Equation (4-50) is integrated with respect to $\ln(\omega)$. The result, with the notation given by Equation (4-43), is then

$$\ln \rho_A = \int \left[ \frac{4}{\pi} \varphi(\ln \omega) - 1 \right] d(\ln \omega) + 2 \int \psi(\ln \omega) \, d(\ln \omega) + c \quad (4-51)$$

where again c is the constant of integration.

An intuitive feeling for the shape of the apparent resistivity function as derived from the phase of the impedance may be obtained by examining the first order term of Equation (4-50). The function defining the slope of $\ln(\rho_A)$ vs. $\ln(\omega)$ for this first order term is depicted in Figure 4-2.

For cases when the phase of the impedance lies between 0 and $\pi/2$ radians, the slope of the $\ln \rho_A$ vs. $\ln \omega$ curve is constrained between -1 and +1. The use of the information contained in Figure 4-2 is sometimes useful in evaluating the data as they are acquired. The basic shape of the apparent resistivity function for given phase
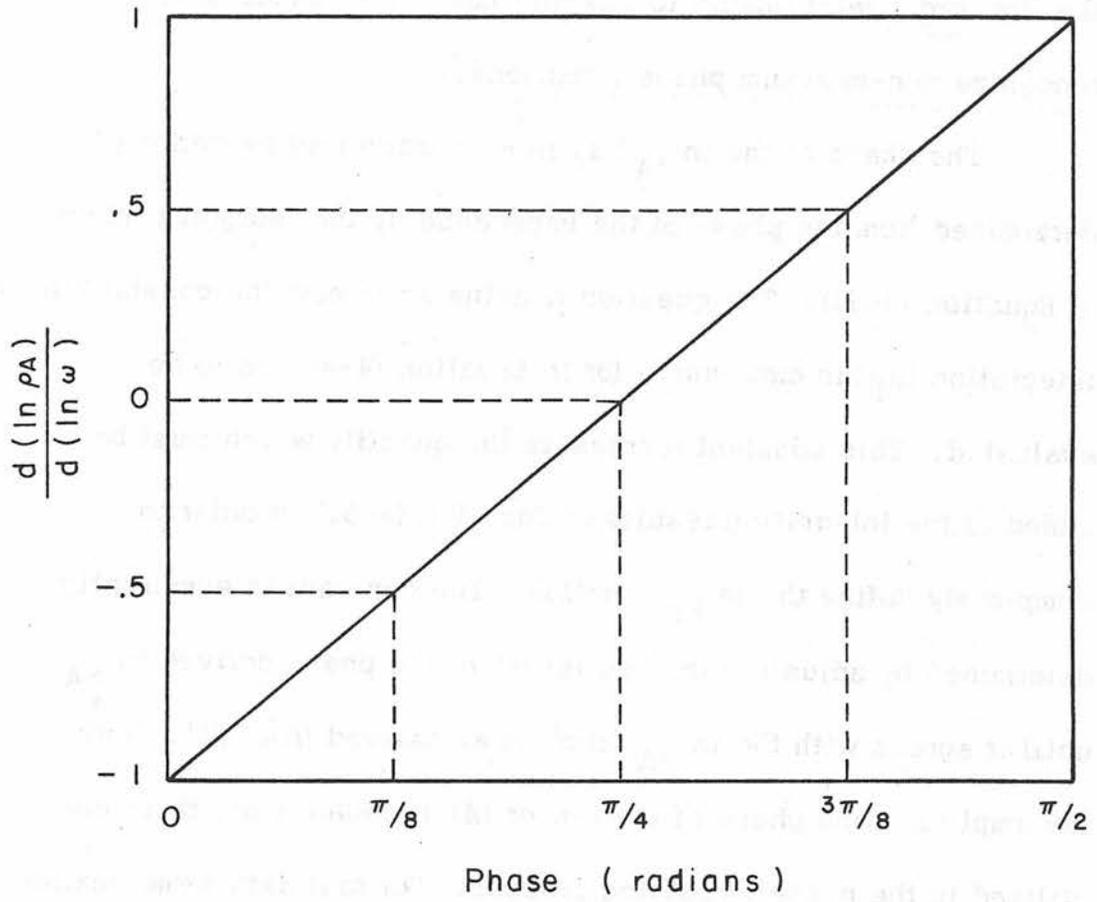
Fig. 4-2. FIRST ORDER PHASE SMOOTHING FUNCTION

information is easily visualized from the first order term. As data at a sequence of frequencies unfold in the field, one can often utilize the first order relationship to pinpoint noisy data bands or to recognize non-minimum phase situations.

The shape of the ln $\rho_A$ vs. ln $\omega$ function may be entirely determined from the phase of the impedance by the integral portion of Equation (4-51). The question remains as to how the constant of integration in this expression (or in Equation (4-46)) is to be evaluated. This constant represents the quantity which must be added to the integration results of Equation (4-51) in order to completely define the ln $\rho_A$ function. The constant is essentially determined by adjusting the "dc level" of the phase derived in $\rho_A$ until it agrees with the ln $\rho_A$ function as derived from $|Z|$. Both the amplitude and phase of the tensor MT impedance are therefore utilized in the phase smoothing process. For real data some scatter will exist on the amplitude points so that the constant is actually determined by adjusting the level of the phase derived curve until a minimum mean square error is achieved with the amplitude data. In practice the least square fit procedure is actually modified to a degree by the coherency of the data points. This will be outlined in Chapter 6.

## V. THE INVERSE FILTER AND NOISE

### A. Signal and Noise Spectra

When the forward going problem of deriving $\rho_A(\omega)$ from the true resistivity vs. depth function is considered, it is found that the relationship between these two functions is in effect a low pass filter operation (Sims and Bostick, 1969). Although the actual resistivity for a layered earth model may be represented by a series of step functions of different amplitudes, the resulting apparent resistivity will appear to be rather smoothly varying as a function of $\ln \omega$. This is not to say that there is no information in the upper portion of the $\rho_A$ spectra which is related to fine earth structure. However, it does mean that this information is given by rapid changes in $\rho_A(\omega)$ which are extremely small. When the variations in the $\rho_A$ data fall below the existing noise level of the MT system, little information about the fine structure of the earth is available for analysis.

If $R_A(x)$ and $R(x)$ are the Fourier transforms of the apparent resistivity and true resistivity, respectively, let the function relating these two quantities be defined as $D(x)$ such that

$$R_A(x) = D(x) R(x). \tag{5-1}$$

Work currently in progress in this laboratory has resulted in an approximate expression for the function $D(x)$. If a one dimensional earth model is considered and certain equations are linearized, it is found that the magnitude of $D(x)$ is given by

$$|D(x)|^2 = \frac{(\pi x)\ \cosh^2\left(\frac{\pi x}{4}\right)}{\sinh\ (\pi x)} \ . \tag{5-2}$$

If the true resistivity function is thought of as a random variable with a flat spectrum then the $\ln\ \rho_A$ transform has the form of

$$R_A(x) = \frac{(\pi x)^{\frac{1}{2}}\ \cosh\left(\frac{\pi x}{4}\right)}{[\sinh\ (\pi x)]^{\frac{1}{2}}} \ . \tag{5-3}$$

As given by Equation (4-28) the transfer function relating the transform of the slope of $\ln\ |Z|$ vs. $\ln\ \omega$ and the phase is

$$S(x) = \pi\ \frac{\Phi(x)}{F(x)} \ . \tag{5-4}$$

The derivative of $\ln\ \rho_A$ with respect to $\ln\ \omega$ is then given by

$$S'_\rho(x) = 2\pi\ \frac{\Phi(x)}{F(x)} \tag{5-5}$$

and since

$$S_\rho(x) = xR_A(x) \tag{5-6}$$

the transform of $\ln\ \rho_A$ is

$$R_A(x) = \left[\frac{2\pi}{XF(x)}\right]\Phi(x). \tag{5-7}$$

To simplify the notation, let

$$G(x) = \left[ \frac{2\pi}{XF(x)} \right]^{-1} \tag{5-8}$$

so that

$$R_A(x) = [G(x)]^{-1} \, \Phi(x) \tag{5-9}$$

or

$$\Phi(x) = G(x) \, R_A(x) \tag{5-10}$$

When Equation (4-32) defining $F(x)$ is substituted into Equation (5-8), it is found that

$$G(x) = \tfrac{1}{2} \tanh\left( \frac{\pi x}{2} \right) \tag{5-11}$$

Figure 5-1 shows the filter function $D(x)$ as defined by Equation (5-1) as well as the transfer function $G(x)$. For large $x$ $D(x)$ dies off in proportion to $x e^{-x}$. This observation confirms the statement made previously that this function is in effect a low pass filter operation. As the value of $x$ decreases the function $G(x)$ becomes very nearly proportional to $x$ so that in the region defined by the derivative of the apparent resistivity. Thus in the lower portion of the phase transform an integration process on the phase provides the apparent resistivity function. For large $x$ the $\ln \rho_A$ and phase transforms are directly related as shown in Figure 5-1. The process involved in deriving $\ln \rho_A$ from the phase, both as a function

52
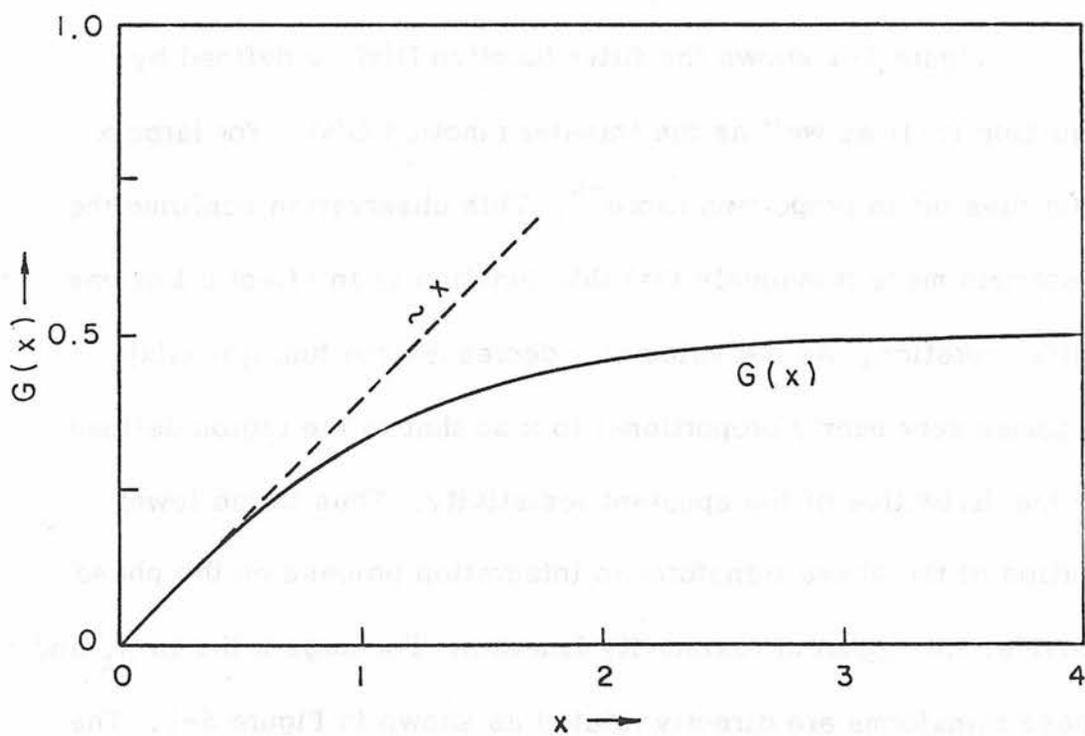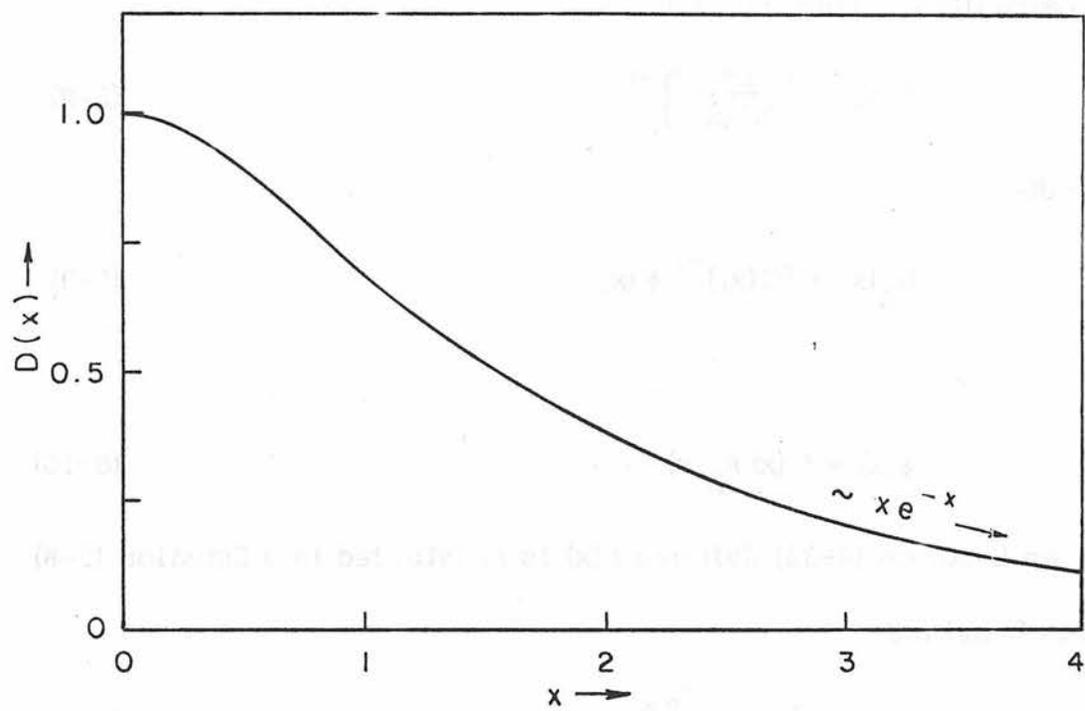


Fig. 5-1. TRANSFER FUNCTIONS D(x) AND G(x)

of ln $\omega$, is depicted in Figure 5-2.

The form of the phase transform is given by the combination of Equations (5-3), (5-10) and (5-11) as

$$\Phi(x) = \frac{\sqrt{(\pi x)}}{2\sqrt{\sinh(\pi x)}} \cosh\left(\frac{\pi x}{4}\right) \tanh\left(\frac{\pi x}{2}\right) \qquad (5-12)$$

The power spectra $|R_A(x)|^2$ and $|\Phi(x)|^2$ of the theoretical ln $\rho_A$ and $\varphi$ signals given by Equations (5-3) and (5-12) are shown in Figure 5-3. In this figure $|\Phi(x)|^2$ has been normalized so that the peak power of this function is unity.

Noise is inevitably encountered in the MT data acquisition process. Let us now assume that white noise exists on the apparent resistivity and phase data as depicted by the dashed lines in Figure 5-3. The transform of both ln $\rho_A$ and $\varphi$ decrease in an inverse exponential manner with respect to the transform variable x for large values of x. Thus there exist points of the MT spectrum above which the noise power exceeds the signal power for ln $\rho_A$ and $\varphi$.

When the signal level of the phase data falls below that of the noise as shown by the point $x_p$ in Figure 5-3 the phase data is for all practical purposes lost and so interpretation of data beyond this point should be curtailed. The function $[G(x)]^{-1}$ of Equation (5-9) used in shaping the apparent resistivity function by the phase information should therefore be modified above the point $x_p$ to include
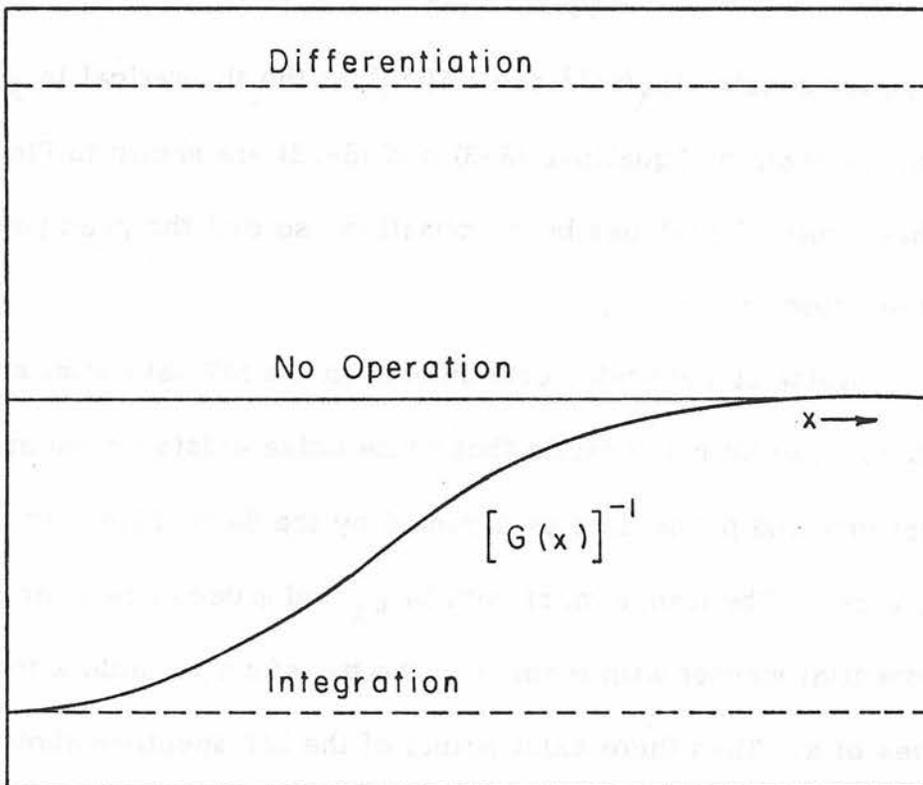
Fig. 5-2. FUNCTION OF THE FILTER $\left[G(x)\right]^{-1}$
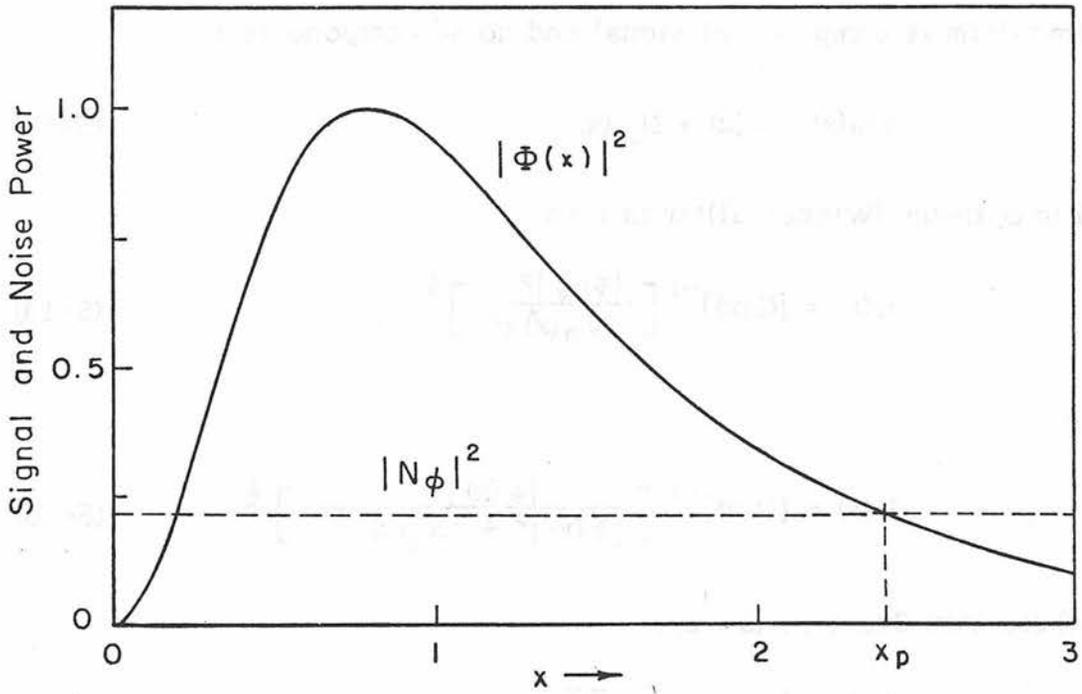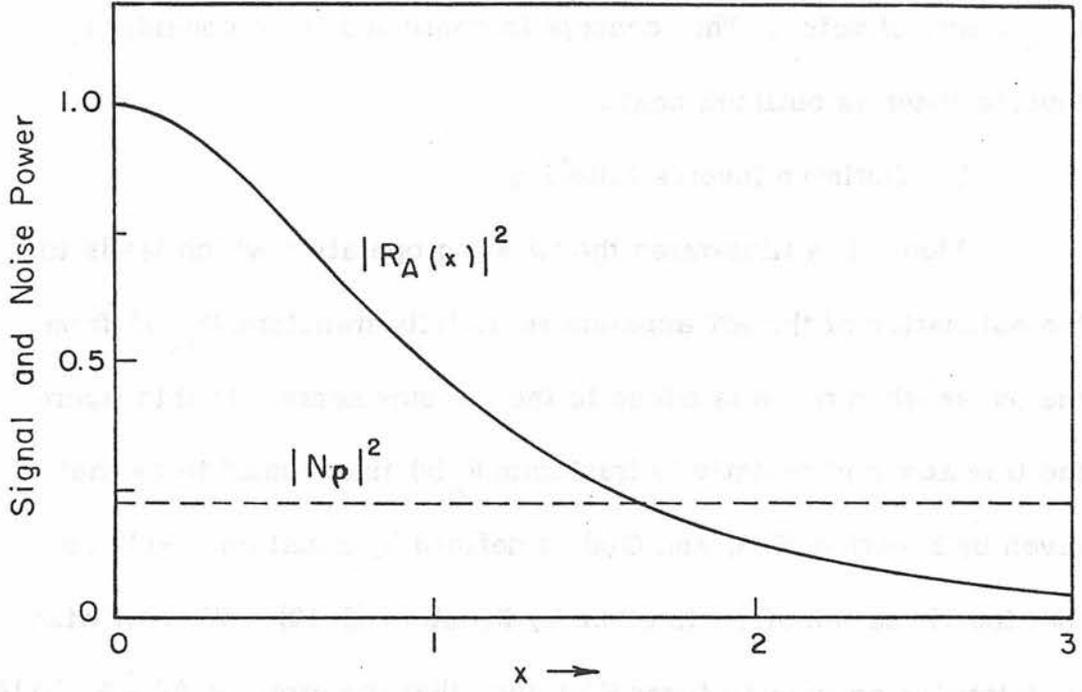
Fig. 5-3. SIGNAL AND NOISE POWER LEVELS

the effects of noise. This concept is confirmed if we consider an inverse filter as outlined next.

B. Optimum Inverse Filtering

Figure 5-4 illustrates the filtering operation which leads to the estimation of the MT apparent resistivity transform $R_{Ae}(x)$ from the phase when noise is added to the measurements. In this figure the true apparent resistivity transform $R_A(x)$ is assumed to be that given by Equation (5-3) and $G(x)$ is defined by Equation (5-11) so that the phase transform is given by Equation (5-12). We now wish to determine an inverse filter $H(x)$ such that the error $|R_A(x) - R_{Ae}(x)|^2$ is minimized for all x. As is shown in Figure 5-4 the measured phase transform is composed of signal and noise components as

$$\Phi m(x) = \Phi(x) + N_\varphi(x).$$ 

<div style="text-align: right">(5-13)</div>

The optimum (Wiener) filter is then

$$H(x) = [G(x)]^{-1} \left[ \frac{|\Phi(x)|^2}{|\Phi_m(x)|^2} \right]^{\frac{1}{2}}$$

<div style="text-align: right">(5-14)</div>

or

$$H(x) = [G(x)]^{-1} \left[ \frac{|\Phi(x)|^2}{|\Phi(x)|^2 + |N_\varphi(x)|^2} \right]^{\frac{1}{2}}$$

<div style="text-align: right">(5-15)</div>

where from Equation (5-12),

$$[G(x)]^{-1} = 2 \coth\left(\frac{\pi x}{2}\right).$$

<div style="text-align: right">(5-16)</div>
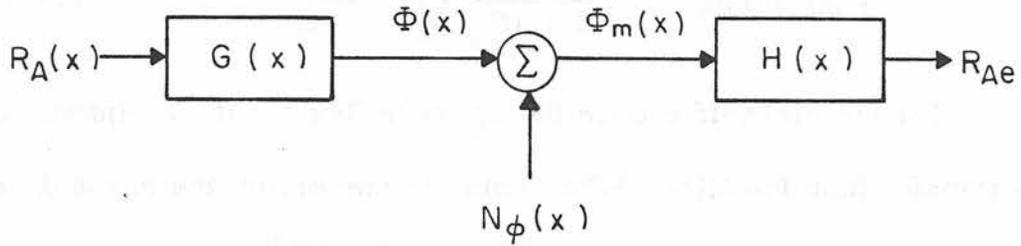
$R_A(x)$ — Actual apparent resistivity

$\Phi(x)$ — Actual phase

$N_\phi(x)$ — Phase measurement noise

$\Phi_m(x)$ — Measured phase

$R_{Ae}(x)$ — Estimated apparent resistivity

Fig. 5-4. INVERSE FILTERING IN THE PRESENCE OF NOISE

An alternate form of H(x) is

$$H(x) = [G(x)]^{-1} \left[ \frac{1}{1 + |N_\varphi(x)|^2 / |\Phi(x)|^2} \right]^{\frac{1}{2}}. \qquad (5\text{-}17)$$

For the noise-free case the optimum filter is the reciprocal of the transfer function $G(x)$. When noise is present on the phase data the optimum filter is a modified version of $[G(x)]^{-1}$. As the signal to noise power ratio decreases an additional filter is applied to $[G(x)]^{-1}$ such that the inverse filter decreases in magnitude from its noise-free form.

As was previously noted, the function $|\Phi(x)|^2$ as shown in Figure 5-3 was normalized so that the peak power of the phase is unity. Figure 5-5 illustrates the optimum filter $H(x)$ for several values of noise power on the normalized $|\Phi(x)|^2$ basis. The roll-off in the inverse filter response indicated when noise is present is done as outlined in the next chapter.
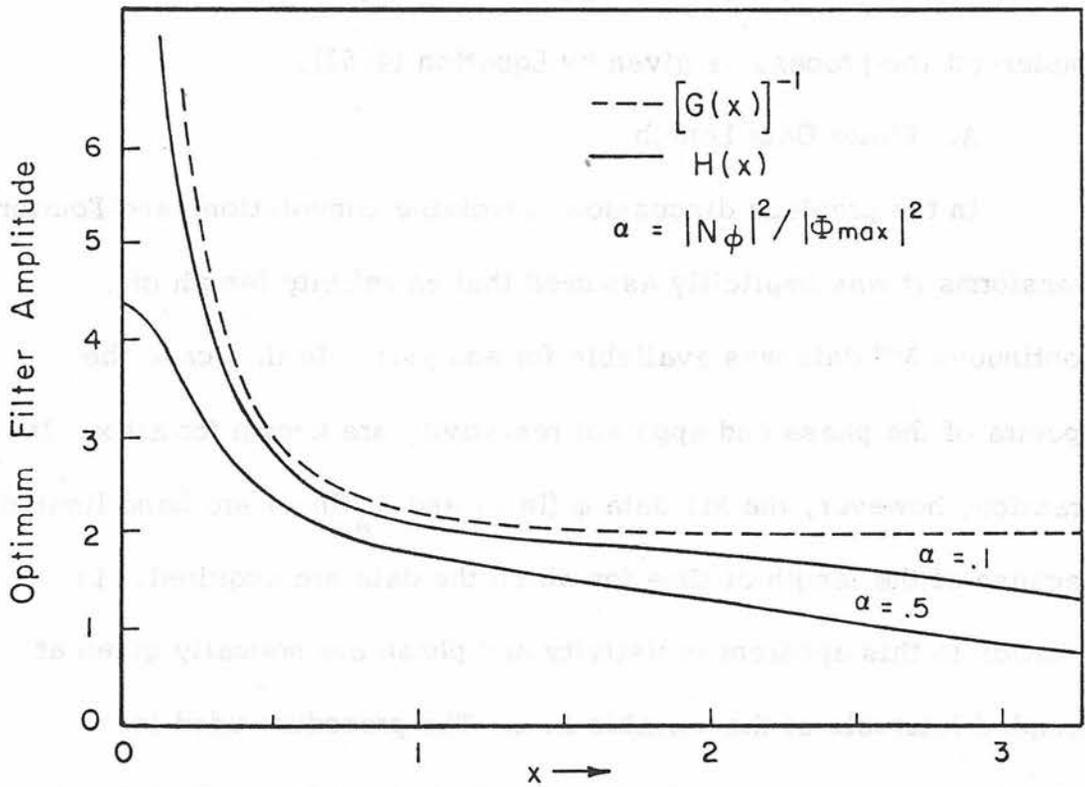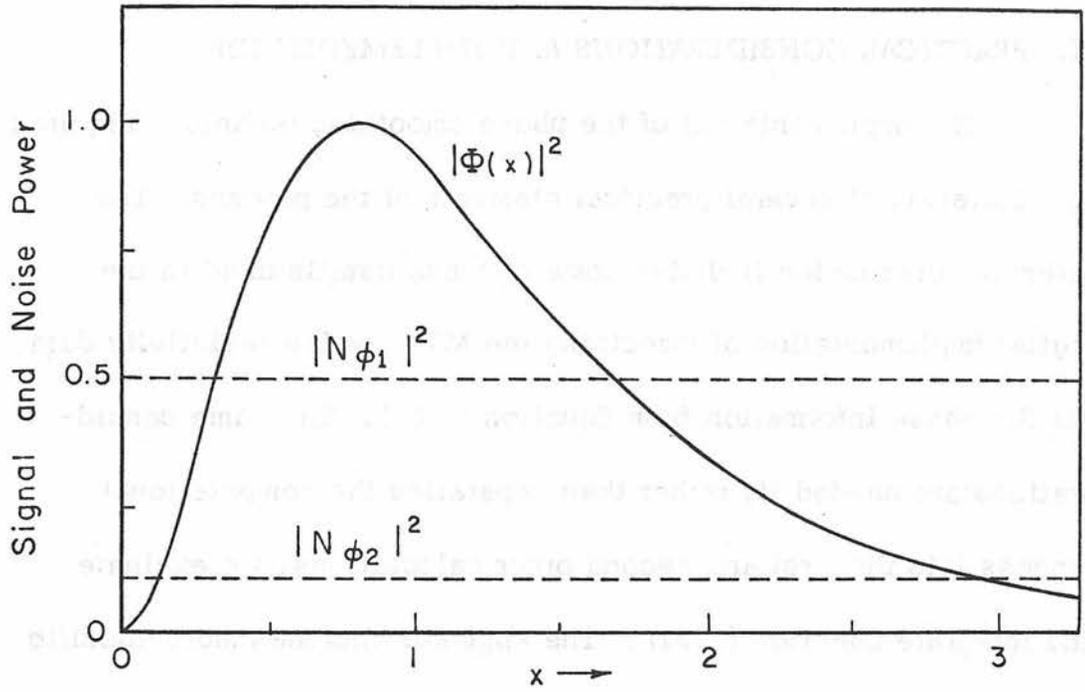
Fig. 5-5. OPTIMUM INVERSE FILTER

VI. PRACTICAL CONSIDERATIONS AND IMPLEMENTATION

The implementation of the phase smoothing technique requires consideration of several practical elements of the process. The following discussion includes some of these details used in the digital implementation of smoothing the MT apparent resistivity data via the phase information from Equation (4-51). The same considerations are needed if, rather than separating the computational process into the first and second order calculations, we evaluate and integrate Equation (4-31). The Appendix includes more specific details regarding a computer program which may be utilized to implement the process as given by Equation (4-51).

A. Finite Data Length

In the previous discussions involving convolutions and Fourier transforms it was implicitly assumed that an infinite length of continuous MT data was available for analysis. In this case the spectra of the phase and apparent resistivity are known for all x. In practice, however, the MT data $\varphi$ (ln $\omega$) and $\rho_A$ (ln $\omega$) are band limited because of the length of time for which the data are acquired. In addition to this apparent resistivity and phase are normally given at sampled intervals of the variable ln $\omega$. The procedure used in calculating the spectra of the MT signals is to utilize a Fast Fourier

60

Transform (FFT) computer routine. This type of computation results in the spectra represented at a series of discrete values of the transform variable x. In order that the FFT may be used, the phase data must be provided at equally spaced ln $\omega$ points. An interpolation routine is used for this purpose as outlined in the appendix.

B. Spectral Content of the Phase

As a consequence of the discussion of Chapter 5, the phase $\varphi(\omega)$ should be well behaved with respect to frequency. That is, any high spectral content in the Fourier transform of $\varphi(\omega)$ are more likely related to noise rather than to the true impedance function. To reduce the effect of this noise, a low pass filtering operation may be applied to the original phase vs. log frequency data. As was pointed out in Chapter 3, if sufficient data are accumulated, the phase of Z is not biased by random noise on the data channels for many cases. The low pass filtering process should result in a curve of $\varphi$ vs. ln $\omega$ which is still unbiased but a smoother version of the original data.

For cases in which only the first order term is to be used to determine the apparent resistivity function, the low pass filter operation is the primary means of reducing the effects of phase noise on the results. Additional modifications to the phase smoothing formulas may be made if the second order term is included.

C. Convolver Width

Even though the convolution indicated in Equations (4-45) or (4-50) is a second order term in these expressions, its contribution to the final resistivity results can be substantial in some instances. This is particularly true if noise is present on the phase data in the upper portion of the spectrum. As was pointed out in the previous chapter there is some point in the spectrum above which the level of the noise power exceeds that of the phase signal (see Figure 5-3). The method currently used to approximate the low pass filter characteristic of the optimum inverse filter is to modify the shape of the convolver used in the evaluation of the second order term.

The Fourier transform $T(x)$ of the convolver function given by Equation (4-44) is shown in Figure 6-1 by the solid curve labeled "A". The low pass function selected to modify $T(x)$ is defined by

$$W(x) = \tfrac{1}{2} + \tfrac{1}{2} \cos\left(\frac{\pi x}{x_f}\right), \quad |x| \leq x_f$$
$$W(x) = 0 \qquad\qquad , \quad |x| > x_f$$

$$(6-1)$$

The resultant convolver transform actually used in Equation (4-50) is shown in Figure 6-1 by the curve labeled "B". The effective width of the convolver may be set in the phase smoothing program by the input parameter $x_f$ (see Appendix for details).
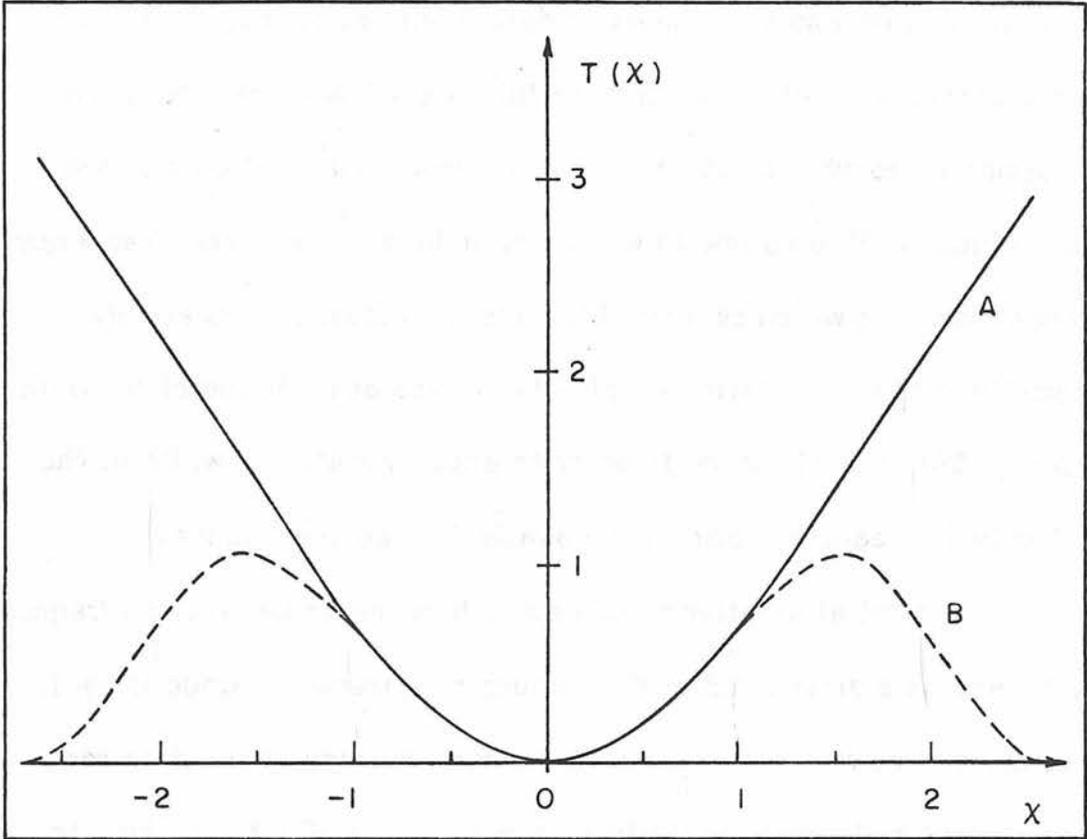
Fig. 6-1. CONVOLVER FUNCTION

D. Convolution End Effects

The phase data $\varphi(\omega)$ is naturally band limited by the sample rate of the data and the number of data points acquired. The need for a convolution with the finite length of $\varphi(\omega)$ obviously raises a question as to what must be done to control the end effects of the convolution. Unless one is willing to reduce the analysis frequency range from that which is available from the actual measurements, some type of extrapolation of $\varphi(\omega)$ is needed at each end of the data range. This must be done in order to accommodate the width of the convolver at each extreme of the available frequency range.

Several alternatives exist as to how the phase vs. log frequency data may be extrapolated at the frequency extremes. Since there is no way of knowing how the phase behaves outside of the data range, one cannot state with authority that one method of extrapolation is superior over any other. It is not claimed that the method used for the examples given subsequently is necessarily the best.

The method used to extrapolate the phase is to extend $\varphi(\omega)$ at each frequency extreme in a linear fashion. In other words the phase in each extended region is assumed to retain the value it had adjacent to these regions as shown in Figure 6-2. One disadvantage of this method is that higher harmonics of phase are introduced into the
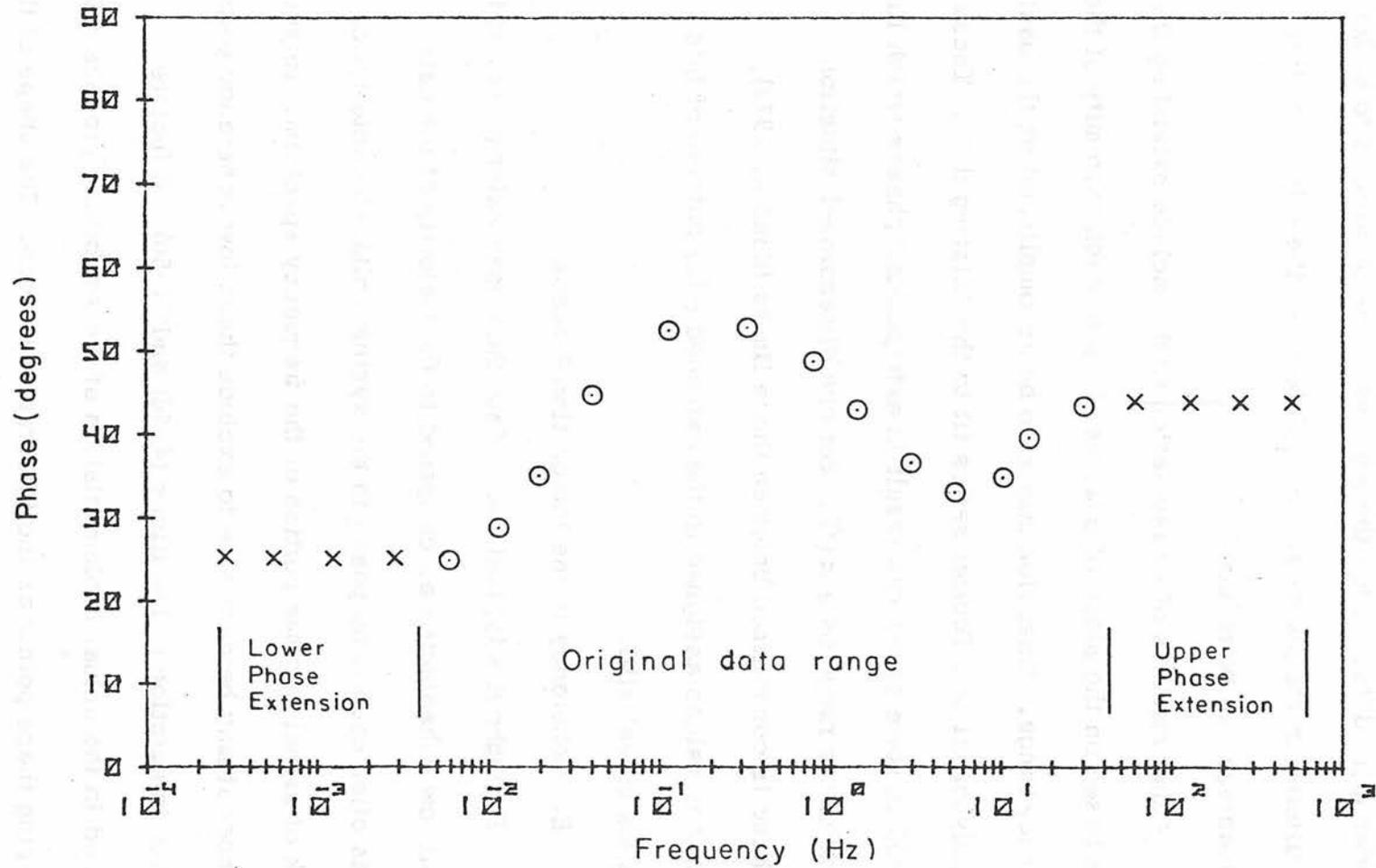
Fig. 6-2. EXTRAPOLATION OF PHASE DATA

extended $\varphi(\omega)$ data. Since the $\varphi(\omega)$ vs. ln $\omega$ function is to be low

pass filtered in the phase smoothing process, the effects of this

disadvantage can be reduced.

Other methods of extrapolation might include extending the

phase based on the slope of $\varphi(\omega)$ vs. ln $\omega$ at each extremity of the

frequency range. Extension may also be accomplished on the basis

of a polynomial or a Fourier series fit to the existing data. These

methods in some cases can result in extrapolated phases which lie

outside of the range $o \leq \varphi \leq \pi/2$. For one dimensional situations

the phase is constrained between these limits (Kunetz, 1972),

and so any values assigned to the extended $\varphi(\omega)$ outside of this

range are unrealistic.

E. Coherency in the Integration Process

Throughout a typical set of data there may exist points which

exhibit low coherencies as compared to the majority of the data.

This is often caused by peaks in the system noise characteristics or

a lack of signal in some portion of the frequency spectrum. In such

instances it may be desirable to exclude these low coherency points

from the integration of Equations (4-46) and (4-50). A feature

included in the actual implementation of the smoothing process allows

bypassing these points as the integration is done. The shape of the

phase derived apparent resistivity curve is therefore not affected by

the phase at frequencies of low coherency data. The minimum coherency included in the actual implementation of the smoothing process allows bypassing these points as the integration is done. The shape of the phase derived apparent resistivity curve is therefore not affected by the phase at frequencies of low coherency data. The minimum coherency level acceptable for the integration process is often variable among different sets of data and so is adjusted according to the overall quality of the particular data set being considered.

F. Evaluation of the Integration Constant

As has been indicated previously, the constant of integration in Equation (4-51) is evaluated by a minimum mean square fit between the phase generated apparent resistivity curve and the original $\rho_A(\omega)$ data. This is accomplished on a log $\rho_A$ basis. The normal least square criterion is modified by the coherency of the data points in this implementation of the phase smoothing process. A brief development of the formula used for this purpose is therefore included here.

The following notation is used in the formulation of the mean square fit for a set of M data points:

$R_i$ = value of $i^{th}$ apparent resistivity point (from measured $|Z|$ )

$A_i$ = value of $i^{th}$ phase derived apparent resistivity point
given by Equation (4-51) (less the constant of
integration)

$C_i$ = coherency of $i^{th}$ data point (as defined in Chapter 3)

L = factor by which each $A_i$ must be multiplied in order
to minimize the error

$\epsilon$ = mean square error.

The standard definition for the mean square error between $R_i$ and $A_i$ on a log basis for N points is

$$\epsilon = \frac{1}{N} \sum_{i=1}^{N} [\log (A_i) - \log (R_i)]^2 .$$ (6-2)

Since each $A_i$ point is to be multiplied by the factor L to yield the minimum mean square error.

$$\epsilon = \frac{1}{N} \sum_{i=1}^{N} [\log (LR_i) - \log (R_i)]^2.$$ (6-3)

It is now desirable to include the effects of coherency in the mean square fit. When noise is present on the $i^{th}$ data point, the amplitude $R_i$ is likely to deviate from its true value. This situation in turn is indicated by a low coherency value $C_i$. In general, the higher the coherency, the more reliable is the data point $R_i$. If some points in the data set are of higher quality than others, it is reasonable to attach more importance to the high coherency points when evaluating the constant of integration. For this purpose let the mean square error of Equation (6-3) be redefined as

$$\epsilon = \frac{1}{N} \sum_{i=1}^{N} \{ C_i^2 [\log (L) + \log (A_i) - \log (R_i)]^2 \} . \qquad (6\text{-}4)$$

It can be seen from Equation (6-4) that the error from the difference in the logarithms of $A_i$ and $R_i$ is weighted more heavily for the higher coherency points. Likewise as the value of $C_i$ decreases, less emphasis is given to the error.

The error is then minimum with respect to log (L) when

$$\frac{\partial \epsilon}{\partial (\log L)} = \frac{2}{N} \sum_{i=1}^{N} \{ C_i^2 [\log (L) + \log (A_i) - \log (R_i)] \} = 0 \qquad (6\text{-}5)$$

or

$$\log (L) \sum_{i=1}^{N} C_i^2 = \sum_{i=1}^{N} \{ [\log (R_i) - \log (A_i)] C_i^2 \} \qquad (6\text{-}6)$$

so that the constant of integration of Equation (4-51) is equivalent to multiplying each $A_i$ by the factor L as given by

$$L = \log^{-1} \frac{\sum_{i=1}^{N} \{ \log (R_i) - \log (A_i)] C_i^2 \}}{\sum_{i=1}^{N} (C_i)^2} . \qquad (6\text{-}7)$$

VII. EXAMPLES OF RESULTS

The phase smoothing process has been used for several years by this laboratory. Included in this chapter are a few examples of the results obtained from this process. These examples include some results of the smoothing technique as applied to synthetic data for a theoretical earth model. Also included are some results from field data.

A. A Model Study

In order to verify that the phase smoothing process may be used in a practical manner, model data with and without noise were utilized in the computer smoothing program. The procedure followed in arriving at the results presented here is as follows.

1. The resistivity vs. depth parameters for a one dimensional earth model were selected. For the example which is shown here a four layered model was used. The constants associated with the layers for this model are listed in Table 7-1 where $\rho$ is the resistivity and T is the thickness of each layer.

| Layer | ρ(ohm-m) | T(km) |
|-------|----------|-------|
| 1 | 360 | 0.42 |
| 2 | 17 | 2.40 |
| 3 | 600 | 11.80 |
| 4 | 5.7 | ∞ |

Table 7-1. Model Parameters

2. Having selected a model, the next step was to generate the synthetic data to be used during the analysis. The complex $H_x$ and $H_y$ source field spectra were defined by a sequence of random numbers generated by a computer routine. This was done for a series of frequencies equally spaced in a linear fashion as if the spectral quantities were output from a Fast Fourier Transform (FFT) routine. The amplitudes of the magnetic field spectra were then additionally shaped to provide data which have the nature of that encountered in the field.

3. The electric field spectra were computed from artificial H data and the model parameters. This was accomplished by applying the forward going problem of a magnetic field plane wave incident on a one dimensional earth with the homogeneous layers as tabulated above. As the propagation characteristics and reflection coefficients are progressively computed from the lowest layer to the top, the surface E field may be determined.

4. The E and H spectra were used in a rather standard Mt
analysis process. This procedure has been used in the past by this
laboratory (Word, et. al., 1970). The various auto and cross
spectra terms needed for the computation of the tensor impedance
estimates were calculated for each frequency used. These terms
were then averaged over a series of constant Q frequency bands to
yield the estimated value of each product at the center frequencies
of each band. The 25.9% bandwidth used results in 10 data points
per decade of frequency equally spaced on a logarithmic scale. The
four estimates of $Z_{xy}$ as given in Chapter 3 were then computed as a
function of frequency. The geometric mean of the amplitudes $|Z|$ and
the average of the phases $\varphi$ of the estimates were next used to define
the complex mean $Z_{xy}$ vs. frequency function.

5. The first example considered in the model exercise was
the application of the phase smoothing process to noise free data.
For this case the $|Z|$ and $\varphi$ functions derived in step 4 above were
used as inputs to the smoothing program. The results of this example
are given in Figure 7-1. The continuous line curve in this figure
represents the apparent resistivity function as computed from the
model parameters. The points plotted as circles show the phase
derived $\rho_A$ function. As can be seen there is very little difference
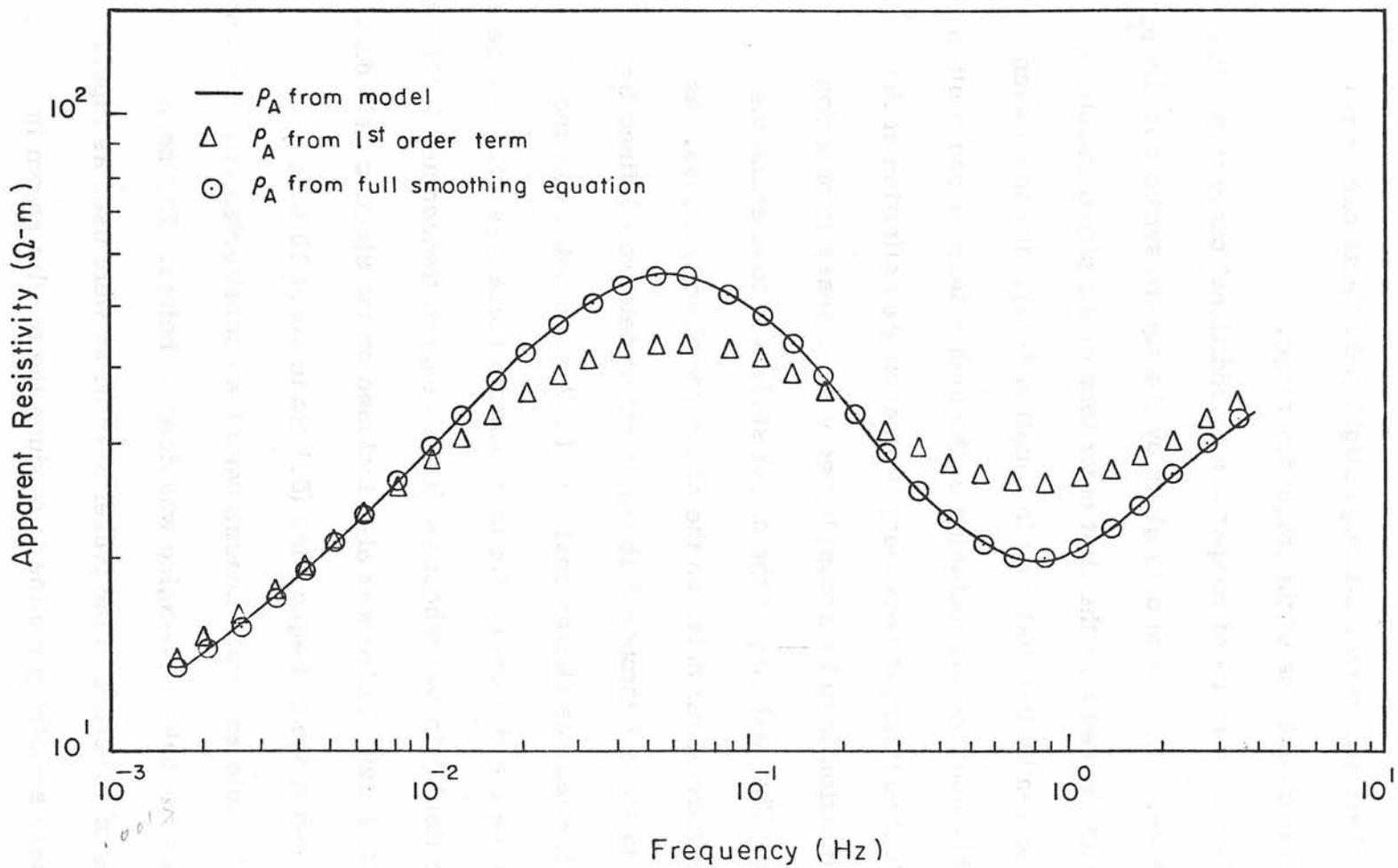
Fig. 7-1. APPARENT RESISTIVITIES FOR NOISE-FREE MODEL DATA

between these two curves although slight end effects can be per-
ceived at each extreme of the frequency range.

For the purpose of comparison an additional curve is plotted
in Figure 7-1. The set of data given by the square symbols is the $\rho_A$
function as derived from the first order term of the phase smoothing
process (given by the first term in Equation 4-51). It can be seen
that in this instance the inclusion of the higher order or convolution
term in that equation is necessary if an accurate definition of the
true $\rho_A$ function is to be accomplished via the phase information.

6. The next step in the model study was to examine the
effects of theoretical noise on the phase smoothing process. As
outlined in steps 1 through 3 above, a set of data was defined for
the four layered one dimensional model. Random noise was then
added to the E and H data. For this example noise was added to the
magnetic field data throughout the lower range of frequencies (.001 Hz
to about 0.1 Hz). Noise was also included on the electric field data
for the upper range of frequencies (0.1 Hz to about 10 Hz).

The auto and cross spectra were then constructed and constant
percentage bandwidth averaging was done as before. The mean
estimates of $|Z|$ and $\varphi$ in the presence of noise were used as inputs
to the phase smoothing routine to produce the results shown in
Figure 7-2. The solid line plot in this figure once again represents
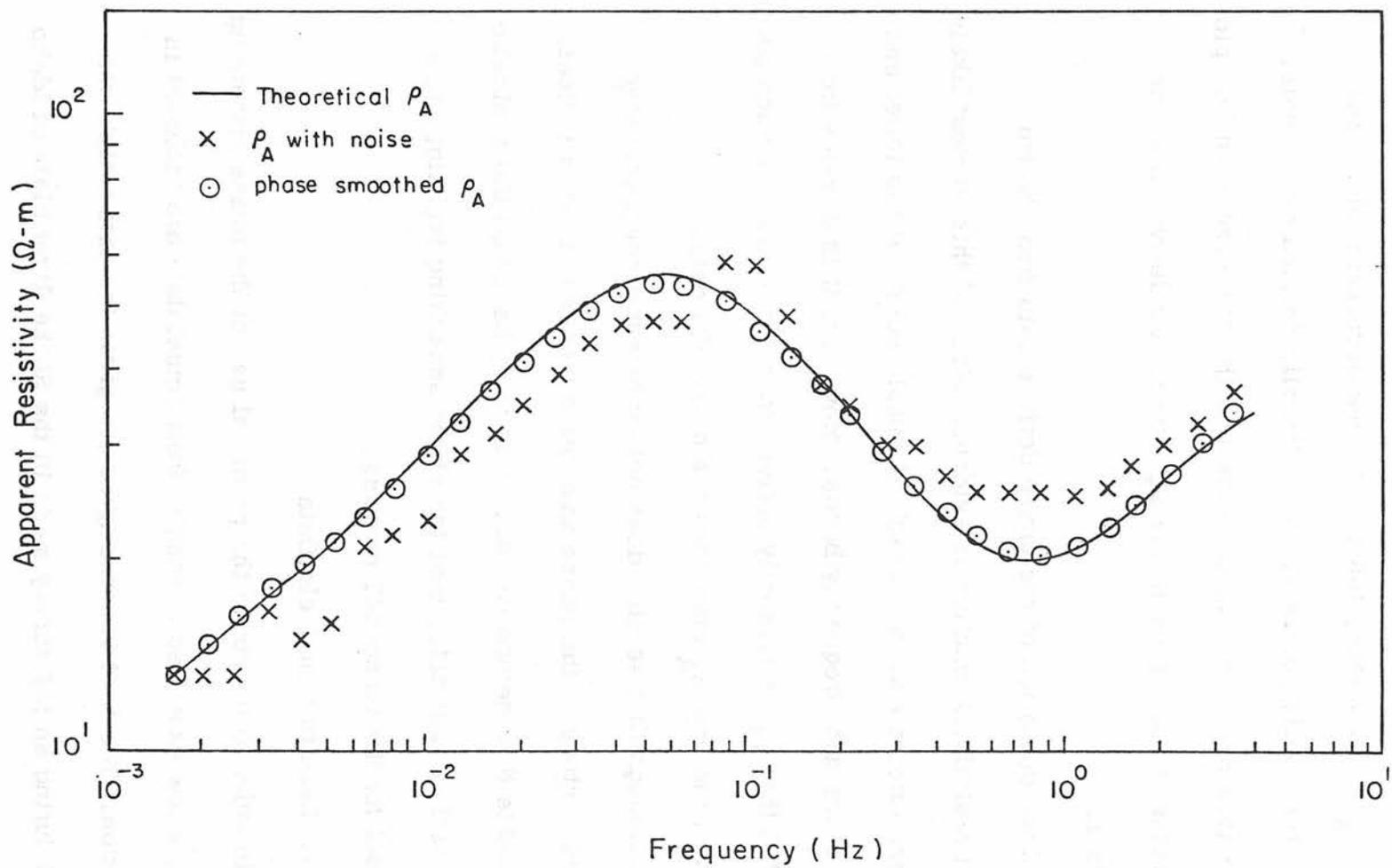
Fig. 7-2. APPARENT RESISTIVITY FOR NOISY MODEL DATA

the true $\rho_A$ vs. frequency function for the assumed model. The apparent resistivity points as conventionally defined by the noisy $|Z|$ data (see Equation 2-7) are shown by the "X" symbol on this plot. The circular symbols present the $\rho_A$ function as derived from the phase data.

Some deviation of the phase derived data from the true apparent resistivity function is evident. Much of this is most likely due to end effects and to the lack of sample points at the lower end of each of the data frequency bands. However, it is obvious from Figure 7-2 that $\rho_A$ as primarily derived from phase gives a much better estimate of the true $\rho_A$ than does the noisy $|Z|$ data.

Although this section does not represent a comprehensive model noise study of the phase smoothing process, it does indicate how valuable this method can be. It is felt, based on the synthetic data as well as real data, that the phase smoothing technique is a useful tool for the tensor MT process.

B. Results from Field Data

In order to illustrate the practical use of the phase smoothing process, a few examples of results from actual data are included in this section. The first two examples are given for data which were acquired during an MT survey made in the Snake River Plain of Idaho

(Stanley, et. al., 1977). The broadband MT data shown in Figure 7-3

for site SR-7 represents points of generally high coherency. The data

for site SR-22 in Figure 7-4 show the results from one of the noisier

data sets used in this survey. In both figures the symbols which are

plotted represent the rotated apparent resistivities $\rho_{xy}$ and $\rho_{yx}$ as

given by Equations (2-7) and (2-8). The solid line curves drawn in

these examples are the phase smoothed functions of these resistivities.

Although the results of only two sites from the Snake River Plain

survey are given here, all the data assembled during this project

were processed in the same manner.

During several months of 1974 this laboratory made a series

of MT sites in northern Wisconsin and upper Michigan (Bostick, et.

al., 1977). Some prototype equipment was used for this project.

A tuneable, phase sensitive Audio Magnetotelluric receiver system

had been designed, constructed, and used in this survey. Because

of the time requirements, little field testing of this equipment was

accomplished before actual measurements were made. Certain un-

anticipated factors encountered through the use of this prototype

equipment resulted in a great deal of noisy data. Some frustration

evolved as the raw apparent resistivity results unfolded throughout

the conventional analyses procedures. It was apparent that these
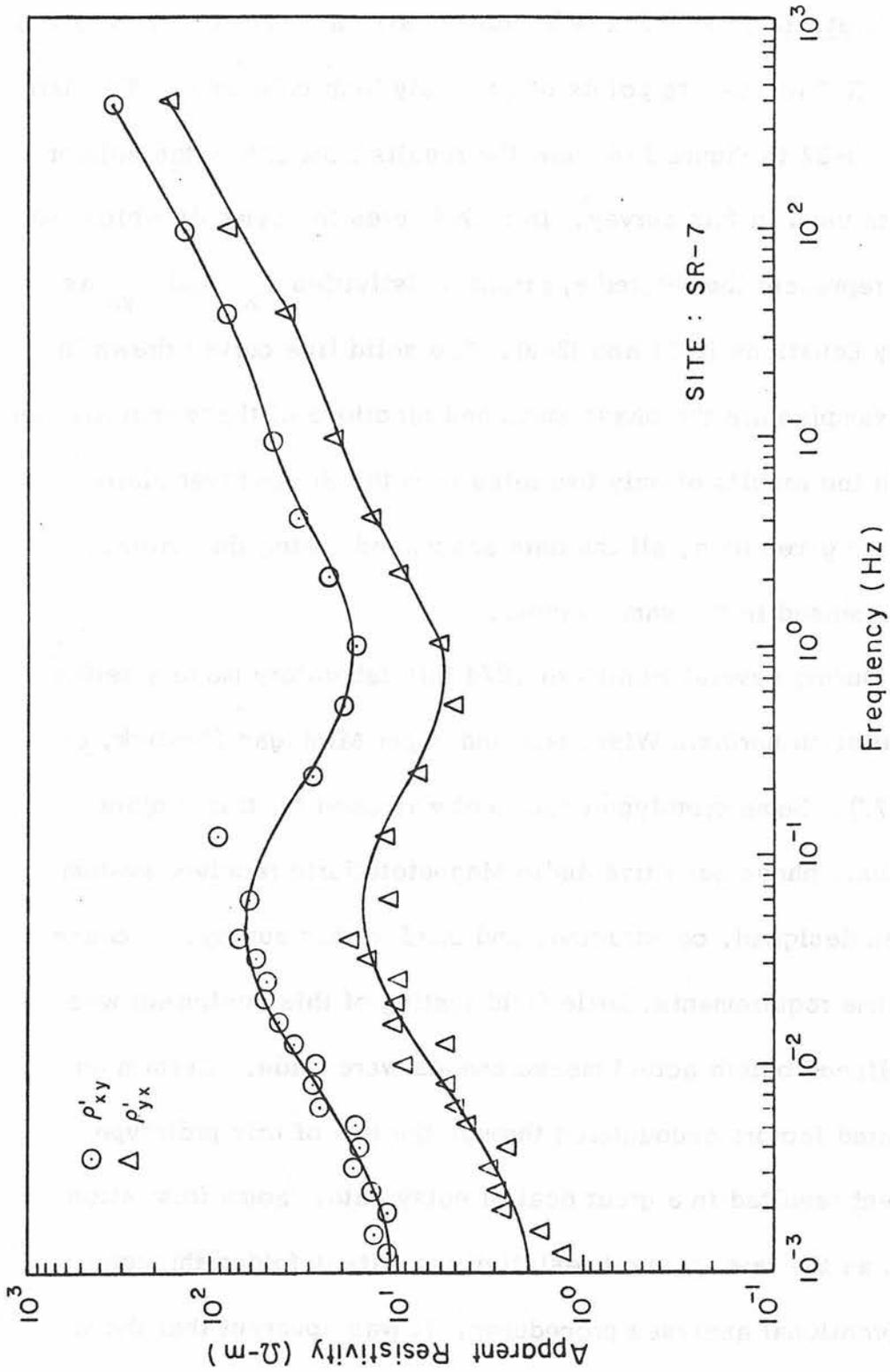
Fig. 7-3. PHASE SMOOTHED RESULTS FOR IDAHO SITE SR-7
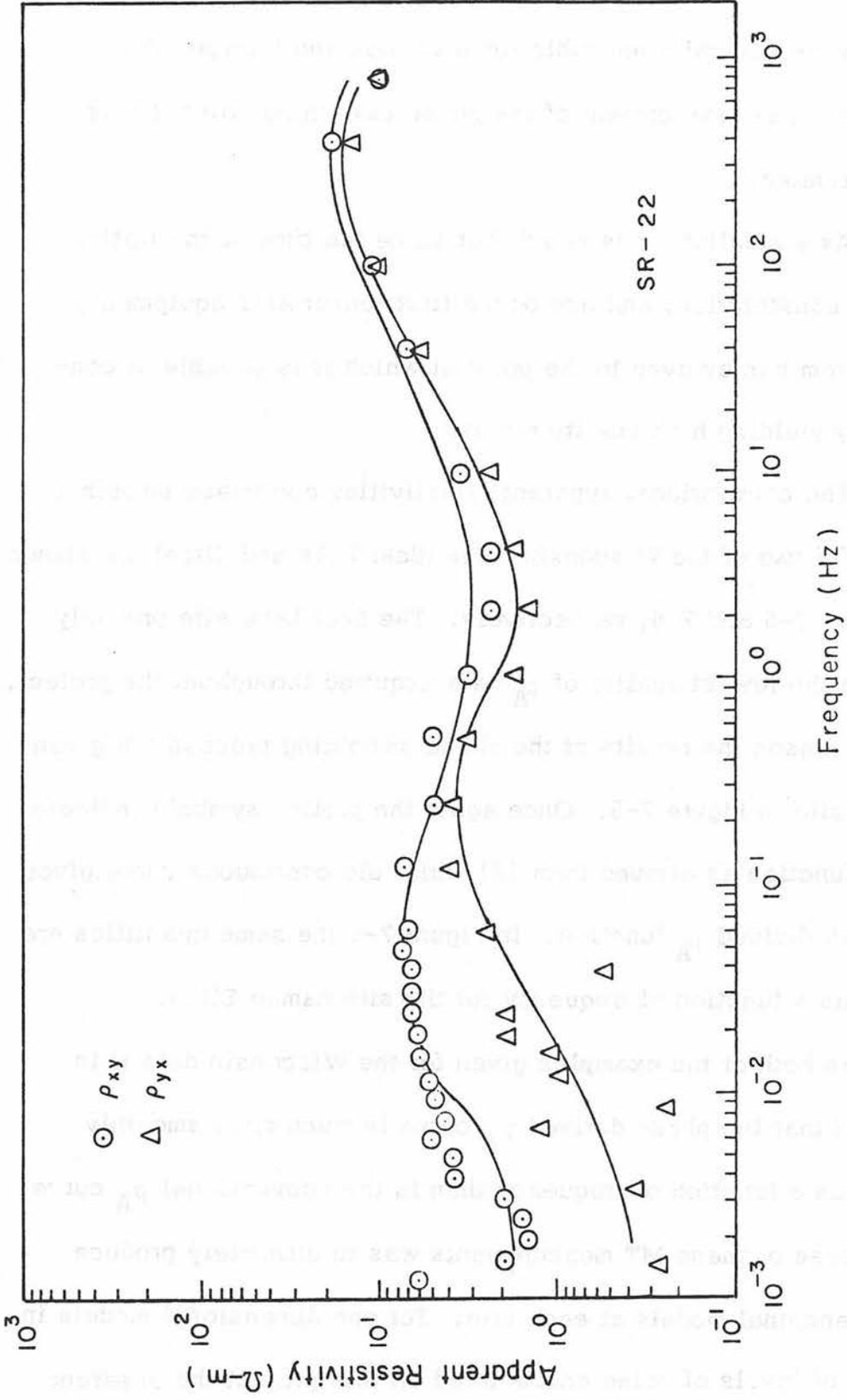
Fig. 7-4. PHASE SMOOTHED RESULTS FOR IDAHO SITE SR-22

results were basically unusable for inversion and interpretation purposes. The development of the phase smoothing process was thus motivated.

As a sidelight it is noted that since the time of the initial design, construction, and use of the first tensor AMT equipment, this system has evolved to the point at which it is capable of consistently yielding high quality results.

The conventional apparent resistivities and phase smoothed results for two of the Wisconsin sites (Bear Lake and Elton) are shown in Figures 7-5 and 7-6, respectively. The Bear Lake site probably presents the lowest quality of $\rho_A$ data acquired throughout the project. For this reason the results of the phase smoothing process are given for this site in Figure 7-5. Once again the plotted symbols indicate the $\rho_A$ function as derived from $|Z|$ while the continuous curve gives the phase derived $\rho_A$ function. In Figure 7-6 the same quantities are plotted as a function of frequency for the site named Elton.

In both of the examples given for the Wisconsin data it is observed that the phase derived $\rho_A$ curve is much more smoothly varying as a function of frequency than is the conventional $\rho_A$ curve. The purpose of these MT measurements was to ultimately produce one dimensional models at each site. For one dimensional models in the face of levels of noise encountered on this project the apparent
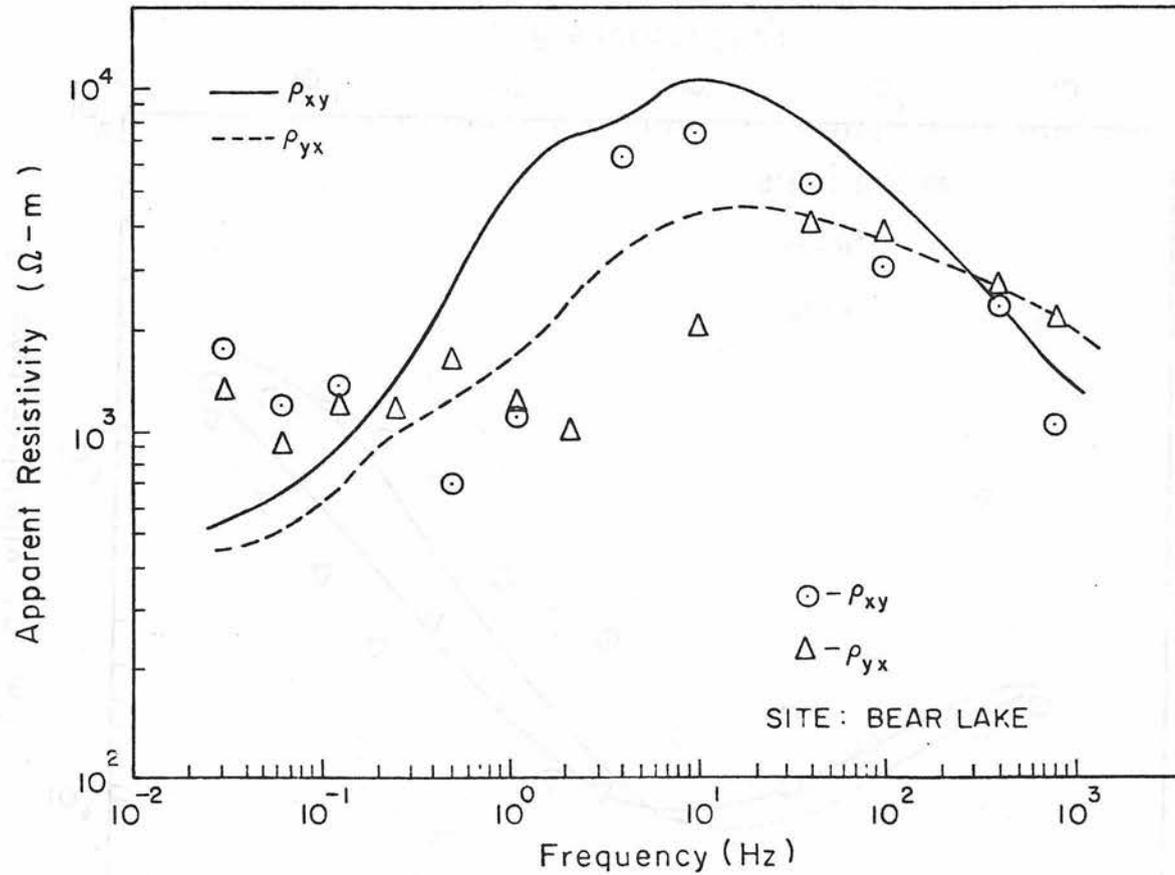
Fig. 7-5. PHASE SMOOTHED RESULTS FOR WISCONSIN BEAR LAKE SITE
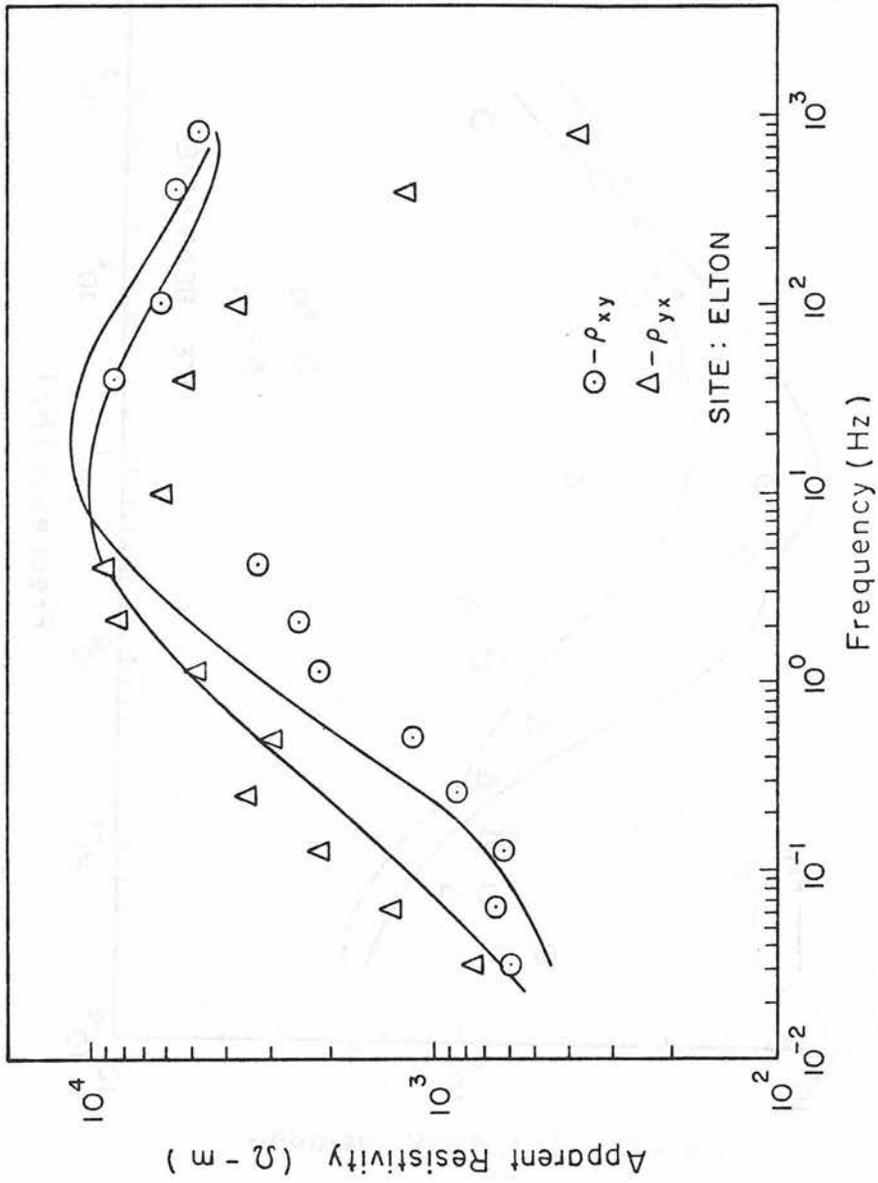
Fig. 7-6. PHASE SMOOTHED RESULTS FROM
WISCONSIN ELTON SITE

resistivity function should vary smoothly with frequency, and so the

phase derived curve would seem to be a more reasonable represen-

tation for $\rho_A$ than that given entirely by the $|Z|$ data.

# VIII. CONCLUSIONS

## A. General

This laboratory has acquired much MT data throughout the past years. During this time a great deal of effort has been expended in attempting to understand some of the subtle causes of noise on the data. Even with the use of the latest generation of MT equipment some scatter is still evident in the raw apparent resistivity results. Of the data accumulated recently much appear to indicate minimum phase conditions for $Z(\omega)$. The phase smoothing has therefore been utilized during the past few years in the MT analysis process.

In some instances when the noise is severe (such as shown in the examples of the preceding chapter), the $\rho_A$ function as given by the measured $|Z|$ data can be essentially uninterpretable. In these cases the phase smoothing technique can prove to be an invaluable aid. Even for non-minimum phase data, however, the technique is useful in providing one dimensional model fits to apparent three dimensional situations. It is therefore felt that the phase smoothing process is a useful tool for the MT analysis method.

Presently the interpretation of MT data is at best a difficult problem. The various inversion techniques are often arbitrarily applied to MT data without an adequate understanding of how noise

can influence these results. Although detailed structure is theoretically available from noise-free data, even a relatively small amount of noise can greatly alter these details when many inversion methods are used. This in turn can result in a false representation of the actual profile encountered. It is therefore felt that, until the noise levels are drastically reduced, apparent subtilties in the raw $\rho_A$ data whould not be interpreted as representing details in the earth's structure.

B. Future Studies Needed

The problem of noise on MT data is an ever present one and deserves a great deal of future consideration. Much needs to be done in the area of understanding to a higher degree the causes and effects of noise on the tensor MT method. Only when all of the mechanisms of noise are comprehended can appropriate steps be taken to minimize their effects.

An efficient means of accurately establishing the character and level of noise present in the measurements at each Mt site would prove very useful. This type of information could be utilized in directly reducing the effects of noise on the data. A knowledge of the noise characteristics can allow the proper selection of one or more estimates for minimum sensitivity to the particular noise. Also, if the noise levels are accurately defined, the expected auto spectra

terms as computed could be modified to reflect the known amount of noise present in the measurements.

A few practical considerations for the use of the phase smoothing process were given in Chapter 6. The details given at that point by no means represent the optimum ways of implementing the process. It may be possible to formulate more efficient methods, and so this could form the basis of future efforts.

# BIBLIOGRAPHY

1.  Becher, W. D., and C. B. Sharpe, A synthesis approach to magnetotelluric exploration, Radio Sci., vol. 4, p. 1089-1094, 1969.

2.  Bode, H. W., Network analysis and feedback amplifier design, D. Van Nostrand, New York, 1945.

3.  Bostick,F.X., Jr., and H. W. Smith, Investigation of large scale inhomogeneities in the earth by the magnetotelluric method, Proc. Radio Eng., vol. 50, no. 11, p. 2339-2346, 1962.

4.  Bostick, F. X., Jr., A simple almost exact method of MT analysis, "Workshop on Evaluation of Electrical Methods in Geothermal Environment," Snowbird, Utah, Nov., 1976, Univ. of Utah Report - Geothermal Workshop, January, 1977.

5.  Bostick, F. X., Jr., H. W. Smith, and J. E. Boehl, Magnetotelluric and dc dipole-dipole soundings in northern Wisconsin, Final Tech. Rep., Electrical Engineering Research Laboratory, Univ. of Texas, Austin, 1977.

6.  Cagniard, L., Basic theory of the magnetotelluric method of geophysical prospecting, Geophysics, vol. 18, no. 3, p. 605-635, July, 1953.

7.  Cantwell, T., Detection and analysis of low frequency magnetotelluric data, Ph.D. thesis, Dept. of Geology and Geophysics, Mass. Inst. of Technology, Cambridge, 1960.

8.  d'Erceville, I., and G. Kunetz, The effect of a fault on the earth's natural electromagnetic field, Geophysics, vol. 27, no. 5, p. 651-665, 1962.

9.  Dowling, F. L., Magnetotelluric measurements across the Wisconsin Arch, Jour. Geophys. Res., vol. 75, no. 14, p. 2683-2698, 1970.

10. Dwight, H. B., Tables of integrals and other mathematical data, The Macmillan Co., New York, 1964.

11. Fischer, G., Symmetry properties of the surface impedance tensor for structures with a vertical plane of symmetry, Geophysics, vol. 40, no. 6, p. 1046-1050, 1975.

12. Geyer, R. G., The effect of a dipping contact on the behavior of the electromagnetic field, Geophysics, vol. 37, no. 2, p. 337-350, 1972.

13. Grosskopf, B. M., F. X. Bostick, Jr., and H. W. Smith, Determination of electric dipole patterns using audio magnetotelluric techniques, Masters thesis, Univ. of Texas, 1974.

14. Guillemin, E. A., The mathematics of circuit analysis, John Wiley and Sons, New York, 1951.

15. Hermance, J. F., Magnetotellurics and geomagnetic deep sounding, EOS, AGU, vol. 52, no. 5, p. 213-216, 1971.

16. Hermance, J. F., Processing of magnetotelluric data, Physics of the earth and planetary interiors, vol. 7, p. 349-364, 1973.

17. Hopkins, G. H., Jr., and H. W. Smith, An investigation of the magnetotelluric method for determining subsurface resistivities, Report 140, Electrical Engineering Research Laboratory, Univ. of Texas, Austin, 1966.

18. Johnson, I. M., and D. E. Smylie, An inverse theory for the calculation of the electrical conductivity of the lower mantle, Geophys. J. Roy. Astron. Soc., vol. 22, p. 41-53, 1970.

19. Kunetz, G., Processing and interpretation of magnetotelluric soundings, Geophysics, vol. 37, no. 6, p. 1005-1021, Dec., 1972.

20. Laird, E. E., and F. X. Bostick, Jr., One-dimensional magneto-telluric modeling techniques, Technical Report 101, Electrical Engineering Research Laboratory, Univ. of Texas, Austin, 1970.

21. Mann, J. E., Jr., A theoretical magnetotelluric problem exhibiting effects of lateral conductivity variations and finite field dimensions, Journ. Geophys. Res., vol. 72, no. 11, p. 2885-2889, 1967.

22. Morrison, H. F., E. Wombwell, and S. H. Ward, Analysis of earth impedances using magnetotelluric fields, Jour. Geophys. Res., vol. 73, no. 8, p. 2769-2778, 1968.

23. Nabetani, S., and D. Rankin, An inverse method of magneto-telluric analysis for a multilayered earth, Geophysics, vol. 34, p. 75-86, 1969.

24. Oppenheim, A. V., and R. W. Schafer, Digital Signal Processing, Prentice Hall, Englewood Cliffs, New Jersey, p. 337-366, 1975.

25. Patrick, F. W., and F. X. Bostick, Jr., Magnetotelluric modeling techniques, Technical Report 59, Electrical Engineering Research Laboratory, Univ. of Texas, Austin, 1969.

26. Price, A. T., The theory of magnetotelluric methods when source field is considered, Jour. Geophys. Res., vol. 67, no. 5, p. 1907-1918, 1962.

27. Rankin, D., The magnetotelluric effect on a dike, Geophysics, vol. 27, no. 5, p. 666-676, 1962.

28. Reddy, I. K., and D. Rankin, Magnetotelluric response of laterally inhomogeneous and anistropic media, Geophysics, vol. 40, no. 6, p. 1035-1045, 1975.

29. Sims, W. E., and F. X. Bostick, Jr., Method of magnetotelluric analysis, Technical Report 58, Electrical Engineering Research Laboratory, Univ. of Texas, Austin, 1969.

30. Sims, W. E., F. X. Bostick, Jr., and H. W. Smith, The estimation of magnetotelluric tensor elements from measured data, Geophysics, vol. 36, no. 5, p. 938-942, 1971.

31. Spitznogle, R. R., Some characteristics of magnetotelluric fields in the Soviet Arctic, Ph. D. dissertation, Univ. of Texas, 1966.

32. Stanley, W. D., J. E. Boehl, F. X. Bostick, Jr., and H. W. Smith, Geothermal significance of magnetotelluric soundings in the Snake River Plain - Yellowstone region, Jour. Geophys. Res., vol. 82, no. 17, p. 2501-2514, 1977.

33. Swift, C. M., Jr., A magnetotelluric investigation of an electrical conductivity anomaly in the southwestern United States, Ph. D. thesis, Geophysics Department, Mass. Inst. of Technology, Cambridge, 1967.

34. Vozoff, K., H. Hasegawa, and R. M. Ellis, Results and limitations of magnetotelluric surveys in simple geologic situations. Geophysics, vol. 28, no. 5, p. 778-792, 1963.

35. Vozoff, K., The magnetotelluric method in the exploration of sedimentary basins, Geophysics, vol. 37, no. 1., p. 98-141, 1972.

36. Wait, J. R., On the relation between telluric currents and the earth's magnetic field. Geophysics, vol. 19, no. 2, p. 281-289, 1954.

37. Weaver, J. T., The electromagnetic field within a discontinuous conductor with reference to geomagnetic micropulsations near a coastline, Canadian Jour. of Phys., vol. 41, p. 484-495, 1963.

38. Word, D. R., H. W. Smith, and F. X. Bostick, Jr., An investigation of the magnetotelluric tensor impedance method, Technical Report 82, Electrical Engineering Research Laboratory, Univ. of Texas, Austin, 1970.

39. Wu, F. T., The inverse problem of magnetotelluric sounding, Geophysics, vol. 33, p. 972-979, 1968.

# APPENDIX

## DETAILS OF IMPLEMENTATION

Figure A-1 illustrates the basic block diagram of the digital computer program which may be used to implement the phase smoothing process.

The input data arrays and program constants are defined as follows:

NPTS – The number of points of the measured apparent resistivity vs. frequency data.

NFREQ – The number of points of data equally spaced on a ln $\omega$ scale to be used in the FFT routine in the convolution process. This parameter must be greater than NPTS and must be equal to an integer power of two.

F – The measured data frequency array.

R(f) – The measured apparent resistivity vs. frequency array.

P(f) – The measured phase data array.

C(f) – The coherency array of the tensor impedance data as a function of frequency.

CMIN – The minimum coherency for which the amplitude data is to be used in the minimum mean square fit process.

U – The constant used in the low pass filtering of the phase data.

91

```
┌─────────────────────────────────────┐
│  Read input data ─ NPTS , NFREQ ,   │
│  F, R(f), P(f), C(f), CMIN, U       │
└─────────────────────────────────────┘
                 │
                 ▼
┌─────────────────────────────────────┐
│  Extend F and P(f) arrays at        │
│  both extremes of data range        │
└─────────────────────────────────────┘
                 │
                 ▼
┌─────────────────────────────────────┐
│  Create an equally spaced ℓn ω      │
│  array over extended range          │
│       with NFREQ points             │
└─────────────────────────────────────┘
                 │
                 ▼
┌─────────────────────────────────────┐
│  Interpolate P(f) data to P(ℓn ω)   │
└─────────────────────────────────────┘
                 │
                 ▼
┌─────────────────────────────────────┐
│  Compute first and second order     │
│    terms  P'(ℓn ω) and Q'(ℓn ω)     │
└─────────────────────────────────────┘
                 │
                 ▼
┌─────────────────────────────────────┐
│  S(log ω) = 4/π [ P'(ℓn ω)+Q'(ℓn ω)] ─1 │
└─────────────────────────────────────┘
                 │
                 ▼
┌─────────────────────────────────────┐
│  Integrate S(log ω) to obtain the   │
│  shape of the phase ─ derived       │
│  apparent resistivity , Y(log ω)    │
└─────────────────────────────────────┘
                 │
                 ▼
┌─────────────────────────────────────┐
│  Interpolate Y(log ω) to            │
│  original data frequencies, A(f)    │
└─────────────────────────────────────┘
                 │
                 ▼
┌─────────────────────────────────────┐
│  Compute constant of integration    │
│  and add to A(f)                    │
└─────────────────────────────────────┘
```

$$S(\log \omega) = \frac{4}{\pi}\left[ P'(\ell n\, \omega) + Q'(\ell n\, \omega)\right] - 1$$

Fig. A-1.   PROGRAM BLOCK DIAGRAM

After the data and program constants have been determined, the phase data is extrapolated at both extremes of the original frequency array as described in Chapter 6.

The derivative of $\ln \rho_A$ as a function of $\ln \omega$ given by Equation (4-50) may be written as

$$\frac{d(\ln \rho_A)}{d(\ln \omega)} = \frac{4}{\pi} \left[ \varphi(\ln \omega) + \mathcal{F}^{-1} \{ T(x) \, \Phi(x) \} \right] - 1 \qquad (A-1)$$

This is the form of the formula which has been implemented via the digital computer program outlined here. For discrete data Equation (A-1) is

$$\frac{\Delta \ln \rho_A}{\Delta \ln \omega} = \frac{4}{\pi} \left[ \varphi(\ln \omega) + \mathcal{F}^{-1} \{ T(x) \, \Phi(x) \} \right] - 1 \qquad (A-2)$$

where the forward and inverse Fourier transforms are computed by an FFT routine.

The MT apparent resistivity function is normally displayed on a log-log scale rather than in terms of the natural logarithm. Since the slope of a function is identical between the two logarithmic bases, Equation (A-2) may be written as

$$S(\log \omega) = \frac{4}{\pi} \left[ P(\ln \omega) + Q(\ln \omega) \right] - 1 \qquad (A-3)$$

where

$$S(\log \omega) = \frac{\Delta \log \rho_A}{\Delta \log \omega} , \qquad\qquad\qquad (A-4)$$

$$P(\ln \omega) = \varphi(\ln \omega) \qquad\qquad\qquad\qquad (A-5)$$

and

$$Q(\ln \omega) = \mathcal{F}^{-1} \{T(x)\ \Phi(x)\} \qquad\qquad\qquad (A-6)$$

Since the transform $\Phi(x)$ in Equation (A-6) is to be computed via an FFT routine, the $\varphi(\ln \omega)$ data must be provided for equally spaced in $\omega$ points. The next step in the program then is to create the equally spaced $\ln \omega$ array over the extended frequency range. The interval between adjacent points is

$$\Delta \ln\omega = \frac{\ln \omega_{NFREQ} - \ln \omega_1}{NFREQ - 1} \qquad\qquad\qquad (A-7)$$

where $\omega_{NFREQ}$ and $\omega_1$ are the upper and lower radian frequency limits, respectively, of the extended range. The number of $\ln \omega$ points (NFREQ) must be an integer power of two for the FFT routine used.

Once the equally spaced $\ln \omega$ array is created, the extended phase array may be interpolated to these points. An existing interpolation routine based on the cubic spline technique was utilized for this process.

As has been discussed, the convolver function $T(x)$ of Equation (4-44) is modified by a low pass filter function. In this

example of the implementation details the phase utilized in the first order term is also low pass filtered to reduce the effect of higher harmonic noise on the phase smoothing results. For purposes of notation let these modifications be denoted in Equation (A-3) as

$$S(\log \omega) = \frac{4}{\pi} [P'(\ln \omega) + Q'(\ln \omega)] - 1 \qquad (A-8)$$

The first and second order terms $P'(\ln \omega)$ and $Q'(\ln \omega)$ of this equation are computed as outlined in Figure A-2.

The values of x for which the FFT routines converts the transform is

$$x_i = i\Delta x, \quad i = 0 \text{ to NFREQ } -1 \qquad (A-9)$$

where

$$\Delta x = \frac{2\pi}{\ln \omega_{NFREQ} - \ln \omega_1} \qquad (A-10)$$

The low pass filter operation illustrated in Figure 6-1 and referred to in the block diagram of Figure A-2 is given by

$$W(x) = \tfrac{1}{2} + \tfrac{1}{2} \cos \left( \frac{\pi x}{x_f} \right) , \quad x \le x_f$$

$$W(x) = 0 \qquad\qquad\qquad , \quad x > x_f \qquad (A-11)$$

and is shown in Figure A-3. The relationship between $x_f$ of this equation and the input parameter U is as follows.

$\Phi(x_i)$ = Fourier Transform of $P(\ln \omega)$

Low pass filter $\Phi(x_i)$ to create $B(x_i)$ array

Apply convolver $T(x_i)$ to $B(x_i)$ to give $D(x_i)$ array

$P'(\ln \omega)$ = Inverse FFT of $B(x_i)$

$Q'(\ln \omega)$ = Inverse FFT of $D(x_i)$
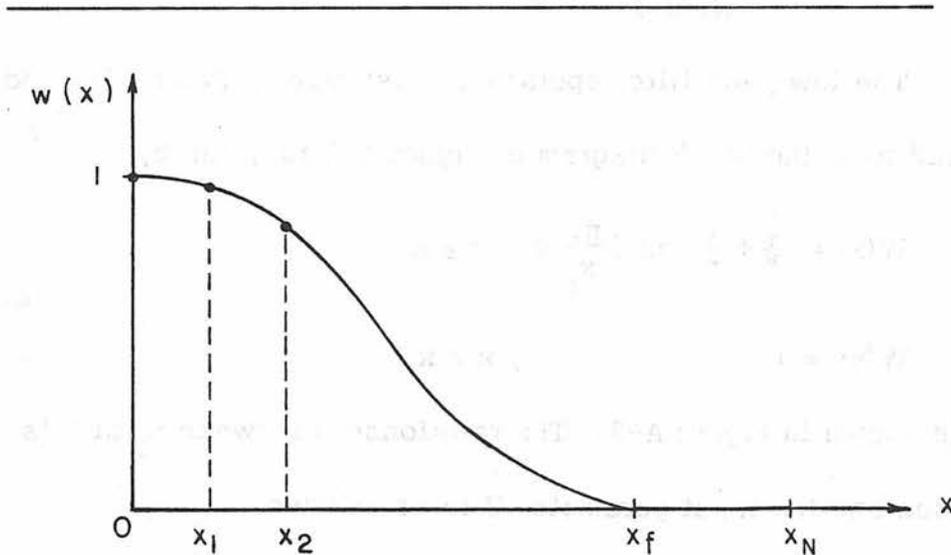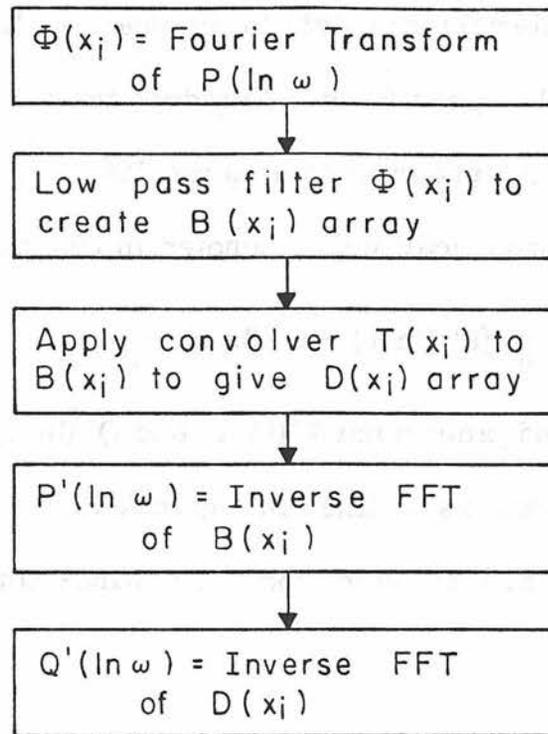


Fig. A-3. W(x) FILTER

Given the phase data at the equally spaced ln ω points we find that the Nyquist point in the x domain is

$$x_N = \frac{\pi}{\Delta \ln \omega} .$$

(A-12)

This point is indicated in Figure A-3. The parameter U is defined as the point on the x axis of this figure given by the fractional part of $x_N$ at which W(x) goes to zero. That is,

$$x_f = U x_N = \frac{U\pi}{\Delta \ln \omega}$$

(A-13)

The low pass filter function is then

$$W(x_i) = \tfrac{1}{2} + \tfrac{1}{2} \cos \left( \frac{x_i \, \Delta \ln \omega}{U} \right) , \; x_i \leq x_f$$

$$W(x_i) = 0 \qquad\qquad\qquad , \; x_i > x_f$$

(A-14)

The transform of the modified phase is then defined as

$$B(x_i) = \Phi(x_i) \, W(x_i)$$

(A-15)

while the transform of the second order term actually used is

$$D(x_i) = T(x_i) \, B(x_i) .$$

(A-16)

where T(x) is defined by Equation (4-44).

After the inverse transforms of $B(x_i)$ and $D(x_i)$ are determined, S(log ω) is computed from Equation (A-8). This step in the program as well as the following are included in the block diagram of Figure A-1.

The next step in the phase smoothing program is to integrate $S(\log \omega)$ to obtain the shape of the apparent resistivity function. The formula used for this purpose is

$$Y_{i+1} = Y_i + \frac{(s_{i+1} + s_i)\, \Delta \log \omega}{2} \qquad (A-17)$$

where $Y_i$ is the log of the $i^{th}$ phase derived apparent resistivity point and the integer i ranges from 1 to NFREQ-1. This iterative process of deriving $Y_{i+1}$ is initiated by assuming any value (0 for instance) for $Y_1$.

There remains the task of evaluating the constant of integration as outlined in Chapter 6. Since the coherencies associated with the original data points are to be used in the evaluation of this constant, the $Y_i$ array derived by Equation (A-17) is interpolated back to the original measurement frequencies. Let this interpolated array be defined as $A_i$, $i = 1, 2, 3, \ldots,$ NPTS. The final phase smoothed apparent resistivity array is then given by

$$A_i = A_i + \log L \qquad (A-18)$$

where L is defined by Equation (6-13).